

# Excessive Long-Time Deflections of Prestressed Box Girders

Prepared by

ZDENĚK P. BAŽANT, QIANG YU, and GUANG-HUA LI

Structural Engineering Report

No. 09-12/ITI

Department of Civil and Environmental Engineering  
McCormick School of Engineering and Applied Science  
Northwestern University  
Evanston, Illinois 60208, USA

**December 2009**

Revised August 31, 2010

# Excessive Long-Time Deflections of Prestressed Box Girders: I. Record-Span Bridge in Palau and Other Paradigms

Zdeněk P. Bažant<sup>1</sup>, Hon. M. ASCE, Qiang Yu<sup>2</sup> and Guang-Hua Li<sup>3</sup>

**Abstract:** The segmental prestressed concrete box girder of Koror-Babeldaob (KB) Bridge in Palau, which had the record span of 241 m (791 ft.), presents a striking paradigm of serviceability loss due to excessive multi-decade deflections. The data required for analysis have recently been released and are here exploited to show how the analysis and design could be improved. Erected segmentally in 1977, this girder developed after 18 years the mid-span deflection of 1.61 m (5.3 ft.), compared with the design camber, and collapsed in 1996 in consequence of remedial prestressing, delayed by 3 months. Compared to three-dimensional analysis, the traditional beam-type analysis of box girder deflections is found to have errors up to 20% (although greater errors are likely for bridges with a higher box width-to-span ratios than the KB Bridge). However, even three-dimensional finite element analysis with step-by-step time integration cannot explain the observed deflections when the current ACI, JSCE, CEB (or CEB-FIP) and GL prediction models for creep and shrinkage are used. These models underestimate the 18-year deflection by 50% to 70% and yield an unrealistic shape of deflection history. They also predict the 18-year prestress loss to be between 22% and 29%, while the measured mean prestress loss was about 50%. Model B3, which is the only theoretically based model, underestimates the 18-year deflection by 42% and gives the prestress loss of 40% when the default parameter values are used. In model B3, however, several input parameters are adjustable and, if they are adjusted according to the long-time tests of Brooks, a close fit of all the measurements is obtained. For early deflections and their extrapolation, it is important that model B3 can capture realistically the differences in the rates of shrinkage and drying creep caused by the differences in the thickness of the walls of cross section. The differences in temperature and possible cracking of top slab also need to be taken into account. Other paradigms on which data have recently been released are four bridges in Japan and one in Czech Republic. Their deflections can also be explained. The detailed method of analysis and the lessons learned are left for part II which follows.

## Introduction

Clarification of the causes of major disasters and serviceability loss has been, and will always be, a prime opportunity for progress in structural engineering. A paradigm that presents such an opportunity for creep and shrinkage analysis and design is offered by the excessive deflections of Koror-Babeldaob (KB) Bridge, which crossed the Toegel Channel between the islands of Koror and Babeldaob in the Republic of Palau in the tropical Western Pacific (Fig. 1a). When completed in 1977, its main span of 241 m (791 ft.) set the world record for segmental prestressed concrete box girders (Yee 1979). The final deflection, measured as a difference from the design camber of  $-0.3$  m (or  $-12$  in.), was expected to terminate at 0.76 to 0.88 m (30 to 34.6 in.), as predicted in design (ABAM 1993, Shawwaf 2008) based on the original CEB-FIP design recommendations (1970-1972). According to the 1971 ACI model (ACI 1971) still in force today (re-approved in 2008; ACI 2008), the deflection (measured from the design camber) would have been predicted as 0.71 m (28 in.) according to McDonald et al. (2003) and 0.737 m (29 in.) according to the present analysis.

---

<sup>1</sup>McCormick Institute Professor and W.P. Murphy Professor of Civil Engineering and Materials Science, Northwestern University, 2145 Sheridan Road, CEE/A135, Evanston, Illinois 60208; z-bazant@northwestern.edu (corresponding author)

<sup>2</sup>Post-doctoral Research Associate, Northwestern University.

<sup>3</sup>Graduate Research Assistant, Northwestern University.

After 18 years, the deflection measured since the end of the construction reached 1.39 m (54.7 in.) and kept growing (ABAM 1993, Berger/ABAM 1995a). The design camber of 0.30 m (12 in.) was not met (Shawwaf 2008) and an additional creep deflection of 0.22 m (9 in.) was accumulated during the segmental erection, making the actual camber only 0.075 m (3 in.) when the cantilevers were joined. Thus the total 18-year deflection at mid-span was 1.61 m (5.3 ft.).

Remedial prestressing was undertaken but caused the bridge to collapse after a 3 month delay, on September 26, 1996, with two fatalities and many injuries (SSFm 1996, Parker 1996, Pilz 1997, 1999, McDonald et al. 2003, Burgoyne and Scantlebury 2006); see Fig. 1b.

As a result of legal litigation, the technical data collected on this major disaster by the investigating agencies have been unavailable to the engineering public for many years. In view of this fact, the first writer, acting in the name of a worldwide group of 47 experts (see Appendix I), proposed at the 3rd Structural Engineers World Congress in Bangalore a resolution which called, on the grounds of engineering ethics, for the release of all the technical data necessary for analyzing major structural collapses, including the bridge in Palau. The resolution passed on November 6, 2007 and was circulated widely. In January 2008, the Attorney General of the Republic of Palau permitted the release of the necessary technical data.

The present two-part study, which updates a 2008 preliminary report (Bažant et al. 2008) and expands a brief recent article (Bažant et al. 2010), aims to explain the reasons for the excessive long-term deflections and compare the performance of various existing models. The method of analysis is presented in detail in part II, which also enunciates the lessons for structural analysis and design. Hopefully, these lessons would resolve the currently intractable disagreements in technical committees about the optimal prediction model for a standard guide. These lessons should also help to interpret the health monitoring of structures. Clarification of the collapse caused by remedial prestressing will be postponed for a later article.

## Bridge Description and Input Data for Analysis

The main span of 241 m (791 ft.) consisted of two symmetric concrete cantilevers connected at mid-span by a horizontally sliding hinge. Each cantilever consisted of 25 cast-in-place segments of depths varying from 14.17 m (46.5 ft.) at the main piers to 3.66 m (12 ft.) at the mid-span. The main span was flanked by 72.2 m (237 ft.) long side spans in which the box girder was partially filled with rock ballast to balance the moment at the main pier. The total length of the bridge was 386 m (1266 ft.). The thickness of the top slab ranged from 432 mm (17 in.) at the main piers to 280 mm (11 in.) at the mid-span. The thickness of the bottom slab varied from 1153 mm (45.4 in.) at the main piers to 178 mm (7 in.) at the mid-span. Compared to the depth of girder, the webs had an unusually small thickness of 356 mm (14 in.), constant through the whole main span. The typical cross sections are shown in Fig. 2.

Type I Portland cement was used for the superstructure (Shawwaf 2008). The mass density of concrete was  $\rho = 2325 \text{ kg/m}^3$  (145 lb/ft.<sup>3</sup>). The top slab was covered by concrete pavement of average thickness 76 mm (3 in.) and density  $2233 \text{ kg/m}^3$  (139 lb/ft.<sup>3</sup>). The aggregate was crushed basalt rock of the maximum aggregate size of about 19 mm (3/4 in.), supplied from a quarry on the island of Malakal. Beach sand from Palau was used as the fine aggregate, and its washing by mechanical means helped to keep the chloride content within the allowed limit (Berger/ABAM 1995b).

Although no original measurements of Young's elastic modulus  $E_c$  of concrete are known, some information was obtained in 1990 by core sample tests (JICA 1990). These tests yielded  $E_c = 22.1 \text{ GPa}$  (3200 ksi). In 1995, further core sample tests (Berger/ABAM 1995a) made just before the retrofit revealed the porosity to be high and  $E_c$  to be about 21.7 GPa (3150 ksi). Both investigations showed values about 23% lower than the value estimated from the design compression strength according to the ACI empirical formula, which is 28.3 GPa (4110 ksi). In JICA's on-site investigation, truck load tests were conducted, and matching the deflections

measured at mid-span by finite element elastic analysis provided, after a correction for concrete age according to the ACI formula, the average 28-day  $E_c$  of about 22.0 GPa, or 3190 ksi (JICA 1990). This is the  $E_c$  value adopted for analysis since the load test gives the average elastic modulus in the box girder.

The prestress was generated by Dywidag threaded alloy bars (tendons) of yield strength 1034 MPa (150 kips) and diameter 31.8 mm (1.25 in.), extended by couplers, anchored by nuts, and grouted in ducts of diameter of 47.6 mm, or 1.9 in. (ABAM 1993, DRC 1996). Some tendons were stressed from one end, some from both (Yee 1979, McDonald et al. 2003). The jacking force of each tendon was 0.60 MN, or 135 kips (DRC 1996). There were 316 tendons above the main pier, densely packed in 4 layers within the top slab. Their combined initial prestressing force was about 190 MN, or 42606 kips (Yee 1979, Pilz 1997, McDonald et al. 2003). The same threaded bars were used to provide vertical prestress in the webs and horizontal transverse prestress in the top slab. The tendon spacing in the webs ranged from 0.3 to 3 m (1 to 10 ft.); Shawwaf 2008. The horizontal transverse tendons in the top slab were spaced at 0.56 m or 22 in. (ABAM 1993, McDonald et al. 2003).

The alloy steel of the tendons had yield strength 1034 MPa (150 ksi) and ultimate strength 1054 MPa, or 153 ksi (DRC 1996). Its Young's elastic modulus was assumed as 200 GPa (29000 ksi) and Poisson's ratio as 0.3. There was also unprestressed steel reinforcement (ABAM 1993), which was taken into account in calculations. In post-collapse examination, neither the prestressed nor the unprestressed steel showed any signs of significant corrosion, despite the tropical marine environment. Some of the ducts, though, showed mild corrosion.

The construction of each segment took slightly more than 1 week (T.Y.Lin International 1996). When the concrete strength in the segment just cast attained 17.2 MPa (2500 psi), 6 to 12 tendons were stressed to 50% of their final jacking force (T.Y.Lin International 1996), and when the concrete strength reached 24.1 MPa (3500 psi), all the tendons terminating in this segment were stressed fully. The segmental erection of the opposite symmetric cantilevers was almost simultaneous and took 6 to 7 months (Yee 1979).

Although the construction was closely monitored, the camber planned to offset the anticipated long-time deflections was not met. The creep and shrinkage during the segmental erection caused an unintended initial sag of 229 mm (9 in.) at mid-span, which could not be corrected during the erection because it would have required abrupt large changes of slope (Shawwaf 2008). The initial sag before installation of the mid-span hinge is included neither in the reported deflection measurements nor in the deflection curves in figures.

The initial deflections for the first two years were benign. However, the longer term deflections came as a surprise. In 1990, the mid-span deflection reached 1.22 m, or 48 in. (JICA 1990), which caused ride discomfort, vibrations after each vehicle passage, and excessive deterioration of the road surface. By 1993 (ABAM 1993), the deflection reached 1.32 m (52 in.). In 1995, just before the removal of roadway pavement (of average thickness of 76 mm, or 3 in.), the mid-span deflection reached 1.39 m (54.7 in.), and was still growing (Berger/ABAM 1995a).

## Creep and Shrinkage Models Considered

As an adequate approximation under service conditions, concrete can be assumed to follow aging linear viscoelasticity with corrections for tensile cracking, variations of humidity and temperature, and drying creep (or Pickett effect). The concrete deformation is then fully characterized by one of the existing prediction models for the shrinkage strain  $\epsilon_{sh}(t)$  and the compliance function  $J(t, t')$ . The prediction models considered in the analysis were the ACI model (ACI 1971, 2008), the CEB (or CEB-FIP, fib) model (fib 1999), the JSCE model (JSCE 1991), the GL model of Gardner and Lockman (Gardner 2000, Gardner and Lockman 2001), and model B3 (Bažant and Baweja 1995, 2000, Bažant and Prasannan 1988, 1989a,b, Jirásek and Bažant 2002). The same computer program using ABAQUS (SIMULIA, Providence, Rhode Island), with the same step-by-step time integration based on Kelvin chain, was used for all

these models (see Part II which follows).

The smallest deviation from the data was obtained with model B3 based on the solidification theory (Bažant and Prasannan 1989a,b), which was first presented in 1995 (Bažant and Baweja 1995), was slightly updated in 2000 (Bažant and Baweja 2000), and was summarized in Jirásek and Bažant's (2002) book. Model B3 represents a refinement of the earlier BP and BP-KX models (Bažant and Panula 1978, Bažant et al. 1991). The theoretical justification was provided in several studies (Bažant et al. 1997, Bažant 2000, 2001). The form of the B3 compliance function for basic creep was theoretically derived and experimentally supported in Bažant and Prasannan (1988, 1989a,b). In statistically unbiased comparisons with the most complete database (Bažant and Li 2008a), model B3 came out as clearly superior to other existing models (Bažant and Li 2008b, Bažant et al. 2008).

The input parameters of the creep and shrinkage prediction models are divided into extrinsic and intrinsic. For all models, the extrinsic parameters, which include the environmental factors, are:

(1) the age at the start of drying, taken here as  $t_c = 7$  days, which is the mean period of the segmental erection cycle ranging from 5 to 10 days (Shawwaf 2008, T.Y. Lin International 1996);

(2) the average environmental humidity  $h = 0.70$ ;

(3) the effective thickness of cross-section  $D = 2V/S$ , to which a minor correction  $k_s$  for body shape is applied in the case of model B3;  $k_s = 1$  for all slabs and webs considered here ( $V/S =$  volume-surface ratio);

(4) for the extended model B3 only, also the temperature.

The intrinsic input parameters, which reflect the composition of concrete, vary from model to model. Formulation of the ACI, CEB and GL models was driven by simplicity, as desired by many engineers. Accordingly, the only important intrinsic parameter in these models is the standard 28-day compression strength  $f'_c$ , while other major influencing parameters such as the cement content and the water-cement and aggregate-cement ratios are not taken into account.

Model B3 is special in that the free intrinsic input parameters are more than one. They introduce the main aspects of concrete composition. If unknown, they can, of course, be set equal to their recommended default values. But their advantage is that one can explore the reasonable ranges of the unknown concrete mix parameters, run the computation of structural response for various plausible sets of values of these parameters, and thus get a picture of the possible range of structural responses to expect. Two sets of input parameters have been considered in computations.

**Set 1:** For simple prediction on the basis of composition, the following input has been used:

(1) The specified compressive strength at 28 days, which is  $f'_c = 35.9$  MPa (5200 psi.) and is the only relatively certain input parameter for the KB Bridge (ABAM 1993). Note that  $f'_c$  is not the required mean strength  $f'_{cr}$  of concrete to be documented by tests during construction. Instead (according to ACI Standard 318, 2008)  $f'_c \approx f'_{cr} - 1.34 \times$  standard deviation (Bažant and Yu 2006). However, in the creep prediction models,  $f'_c$  is used as the input parameter (ACI 2008).

(2) The 28-day elastic modulus, which was not specified in design. The  $E_c$  value measured just before the retrofit is appropriate for Set 2 but must not be used for Set 1, which is intended to check the prediction capability of the model. The only way  $E_c$  could be determined at the time of design was from the approximate ACI formula  $E_c = (57,000 \text{ psi}) \sqrt{f'_c(\text{psi})}$ , which gives  $E_c = 28.3$  GPa (4110 ksi).

(3) Cement content  $c = 26$  lb/ft<sup>3</sup>, aggregate-cement ratio  $a/c = 4$  and water-cement ratio  $w/c = 0.62$  (high  $w/c$  was mentioned in ABAM 1993, and by Shawwaf, 2008, but a precise value was not reported). Based on the B3 empirical formulas estimating the intrinsic parameters from concrete composition (Bažant and Baweja 2000), the result was:

$$q_1 = 0.146, q_2 = 1.04, q_3 = 0.045, q_4 = 0.053, q_5 = 1.97 \quad (\times 10^{-6}/\text{psi}) \quad (1)$$

$$\epsilon_{k\infty} = 0.0013 \quad \text{and} \quad k_t = 19.2 \quad (\text{Set 1}) \quad (2)$$

**Set 2 (updated):** For a better estimate, only the values of  $q_2$ ,  $q_5$  and  $\epsilon_{s\infty}$ , governing mainly the response for the first few years, have been estimated from the composition, and the estimates of the remaining parameters were improved as follows:

$$q_1 = 0.188, \quad q_3 = 0.262, \quad q_4 = 0.140 \quad (\times 10^{-6}/\text{psi}) \quad (\text{as changed for Set 2}) \quad (3)$$

where  $q_1$  was adjusted according to the elastic modulus obtained in the truck load test; and  $q_3$  and  $q_4$  were identified by a trial-and-error procedure, conducted with two objectives in mind: (1) stay close to the values of the available creep tests of duration  $\geq 10$  years, which are only three: the 10-year and 30-year tests of Brooks (1984, 2005), the 18-year tests of Russel and Burg, and the 23-year tests of Troxell (Troxell et al. 1958); and (2) obtain the closest possible fit of the measured deflection of the KB Bridge agreeing with these long-time tests. In Fig. 3, it can be seen that the selected intrinsic parameters agree with the 10-year creep tests reasonably well.

It has been noted that compliance function  $J(t, t')$  that agrees with the tests of Brooks, Russell and Burg, and Troxell et al. (which are the only existing tests with durations  $> 10$  years) gives good agreement with the measured deflections. This fact suggests using these tests for recalibrating input parameters  $q_3$  and  $q_4$ , which are in model B3 the main controlling parameters of multi-decade creep and are difficult to estimate from the database since the database is dominated by test data for load durations  $< 5$  years.

To calculate and compare the predictions of various models, all the properties of concrete and environmental histories of the KB Bridge concrete would have to be known. But they are not. So, comparing the predictions of various models either mutually or with the observations is not fully informative. Nevertheless, what can be compared is whether the observed deflections are within the realistic range of each model. They are indeed seen to be within the realistic range for model B3, but not at all for other models, including the ACI, CEB, JSCE and GL models.

For model B3, the predictions are not fixed because there exist input parameters that are for the KB Bridge unavailable and are thus free to set within their realistic range. But the predictions of the other models are fixed by the reported value of concrete strength, with no flexibility of adjustment (a partial exception is the JSCE model, which takes into account the water content  $w$  and cement content  $c$ ). The data available for the KB Bridge, as presented here, do not suffice to obtain for this bridge a unique compliance function (unless the default parameter values are used). But they do suffice to obtain unique compliance functions for the ACI, CEB, JSCE and GL models, although at the cost of ignoring many important influences.

Some engineers desire the model to predict creep and shrinkage from as few parameters as possible, particularly from the concrete design strength only (ACI 2008). More convenient though it might be, realistic it is not. If the additional parameters of model B3 for the given concrete are known, better prediction can be made. If they are unknown, they can be assigned their typical, or default, values, and thus predictions can still be made even if only the strength is known. Furthermore, varying the influencing parameters of model B3 through their realistic range, one can explore the realistic range of the responses to expect, and design the structure for the most unfavorable realistic combination. With the other models, one can explore only the effect of strength variation.

## Computed Deflections and Prestress Loss, and Comparisons to Measurements

Because of symmetry, only one half of the bridge is analyzed. A three-dimensional finite element program, which automatically captures all the stress-redistribution effects due to creep, is used (see the mesh in Fig. 2). As the first check of the program, a comparison is made with the

bridge stiffness, which was measured in January 1990 in a load test by Japan International Cooperation Agency (JICA 1990). An average downward deflection of 30.5 mm (0.10 ft.) was recorded at mid-span when two 12.5 ton trucks were parked side by side on each side of the mid-span hinge (one previous paper erroneously assumed that only one truck was parked on each side). The front wheels of the two trucks on each side were assumed to have been 3 m away from the mid-span. The rear wheels, 12 m behind the front wheels, were assumed to carry 60% of the truck weight. The finite element code predicted the deflection of 30 mm (0.098 ft.) that was measured approximately within 2.4 hours (the 2.4 hour creep was based on model B3 Set 2) under the load of 245 kN (55.1 kips). Given the uncertainty about the actual rate of loading, the difference is small enough.

The results of calculations are shown in Figs. 4–7, both in linear and logarithmic time scales ( $t - t_1 =$  time measured from the end of construction,  $t_1 =$  time when the mid-span hinge is installed). The data points show the measured values. The circles represent the data reported by the firm that investigated the excessive deflections (JICA 1990), and the diamonds the data accepted from a secondary source (Berger/ABAM 1995). For comparison, the figures show the results obtained with model B3 and the ACI, CEB, JSCE and GL models. All these responses have been computed with the same finite element program and the same step-by-step time integration algorithm. For model B3, it was possible to consider the effect of the differences in thickness of the slabs and webs on their drying rates.

Fig. 4 shows the deflection curves up to the moment of retrofit at about 19 years of age. Since well designed bridges (such as the Brooklyn Bridge) have lasted much longer, Fig. 5 shows the same curves extended up to 150 years under the assumption that there has been no retrofit (and thus no collapse).

Fig. 6 presents the mid-span deflection that is obtained (1) if the drying creep is neglected, (2) if both the shrinkage and drying creep are neglected, and (3) if the shrinkage and the drying creep compliance are considered to be uniform over the cross section and to be deduced from the overall effective thickness  $D = 2V/S$  of the whole cross section. Note that the use of uniform creep and shrinkage properties throughout the cross section neglects the curvature growth due to differential shrinkage and differential drying creep and gives results dominated by the unusually thin webs. Also note that the effect of mean drying can be very different from the mean of the effects of drying in the individual slabs (Bažant et al. 1992).

The shear lag effect (with the associated creep-induced stress redistributions within the cross sections) necessitates three-dimensional simulations. It cannot be realistically captured by the classical concept of effective width of the top slab (which was actually used in the design of the KB Bridge). The computations show that the shear lag occurs in four different ways—in the transmission of vertical shear force due to vertical reaction at the pier, in the transmission of the concentrated forces from tendon anchors, and for each of these in the horizontal slabs and in the vertical walls. Only full three-dimensional analysis can capture this behavior. It always yields larger deflections and larger prestress losses. The beam-type analysis causes, for the bridge in Palau, an error of  $-20\%$  in deflections and  $-10\%$  in the prestress loss (the errors are larger in the 95% confidence limits, discussed later).

Accuracy in calculating the prestress loss is crucial because the bridge deflection is a small difference of two large but uncertain numbers—the downward deflection due to self-weight, and the upward deflection due to prestress. Calculations show that, compared to the classical theory of bending, all the shear lags combined increase the elastic downward deflection due to self-weight by 18% and the elastic upward deflection due to initial prestress by 14%, which jointly produce the aforementioned total shear lag effect of 20%.

The measured deflection at 18 years since span closing, which was 1.39 m, is closely matched by the deflection calculated from model B3 with set 2 parameters. This measured deflection is roughly 3-times larger than that calculated for the ACI or CEB model (which is 0.47 m or 0.53 m), and about the double of that calculated for the GL model (which is 0.65 m); see Fig. 4. Besides, the ACI, CEB, JSCE and GL deflection curves have shapes rather different from those

of model B3 as well as the observed deflection history. They all give far too much deflection growth during the first year, and far too little from 3 years on, especially for the ACI, CEB, and JSCE models.

An important point to note is that the 19-year prestress loss is only 22% and 24% when the ACI and CEB models are used in the present finite element code, but about 46% when model B3 is used (Fig. 7).

The correctness of prestress loss predicted by model B3 is confirmed by stress relief tests which were made by ABAM on 3 tendons just before the retrofit (Berger/ABAM 1995a). Sections of three tendons were bared, and strain gages were glued at 3 different locations on each of the three tendons. Each of these tendons was then cut, and the stress was calculated from the shortening measured by the gage next to the cut; see Table 1. The average stress obtained from 9 measurements on the tendons was 377 MPa (54.7 ksi). This means that the average prestress loss over 19 years was about 50%. The coefficient of variation was 12.3%. Model B3 (set 2) calculations give the prestress loss of 46%, which deviates from the measured mean by only 9%. This is less than the coefficient of variation of these measurements, which was 12.3%. Similar tests were also conducted by another investigating company (Wiss, Janey and Elstner, Highland Park, Illinois) and the average measured prestress loss was almost same.

Normally only nondestructive methods are permitted. This makes it next to impossible to measure the stresses in grouted tendons. But for the KB Bridge the cutting of tendons was not a big sacrifice because additional tendons were to be installed anyway. Thus the decision to retrofit furnished a unique opportunity to learn about the actual prestress losses.

In the mid 1970s, the prestress loss used to be calculated not by finite elements but by simple formulas based on the beam theory (e.g., Nilson 1987). A lump estimate of the final prestress loss was generally used and, according to Shawwaf 2008, it was used for the KB Bridge. According to the lump estimate, the prestress loss would have been 22%, which is marked in Fig. 7 by a horizontal dashed line. Compared to the measurements, the errors of this estimate are enormous, and so are the errors compared to the present calculation based on model B3. These errors are one reason why the long-time deflections were so badly underestimated in design. One must conclude that, for large box girders, the standard textbook formulas for prestress loss are inadequate and dangerously misleading.

According to the ACI, CEB and the JSCE models, the compliance curves and the deflection curves terminate with a horizontal asymptote. But according to model B3, the long-time compliance curves are logarithmic. Thus model B3 predicts the deflection curve to terminate in the logarithmic time scale with an asymptote that is a straight line of a finite slope, which agrees very well with the observations (Fig. 4). However, the final slope predicted by model B3 (Set 1) for 18 years is too small. To match the slope in Fig. 4, it would need to be increased by the factor of 1.52.

For times longer than about 3 years, the deflections are seen to evolve almost linearly in the logarithmic time scale (which is to be expected for theoretical reasons, Bažant 2000), and can thus be extrapolated to longer times graphically; see Fig. 5. The graphical straight-line extrapolation is seen to agree almost exactly with model B3 calculations up to 150 years. It is virtually certain that if the bridge were left standing without any retrofit, the 150-year deflection would have reached 2.24 m (7.35 ft.), well beyond the limit of serviceability.

Capturing correctly the initial deflection history is essential for correct extrapolation, to foresee later troubles. The differential shrinkage and drying creep due to nonuniform drying is important in this respect (Křístek et al. 2005, Křístek et al. 2006, Křístek et al. 2008 ). Note in Fig. 4 that, for the early deflection history, too, model B3 gives by far the closest prediction.

## **Excessive Long-Term Deflections of Other Box Girders**

It is deplorable that the data on excessive deflections usually go unpublished. Nevertheless, Y. Watanabe, the chief engineer of Shimizu Corp., Tokyo, graciously made available the data on

some large Japanese bridges which epitomize the experience in many other countries. These deflection data are plotted in Fig. 8, where the data points represent the measured deflections, and the dashed curves show the prediction based on the design recommendations of Japan Road Association (JRA). The solid curves give the predictions of model B3 calculated in the same way as for the KB Bridge, after adjusting the composition parameters similarly to set 2, as mentioned before.

The foregoing observations document that the deflections of the KB Bridge are not a unique occurrence. Interestingly, one of these four bridges, Urado, does not show excessive 30-year deflection; the reasons may be that the creep curve in the JRA code is set about 60% higher than in the JSCE code. However, the deflection slope at 30 years portends troubles for the future.

The absence of a mid-span hinge has been known to reduce deflections. However, it is not a panacea. Even bridges without a mid-span hinge, designed by the code, can suffer excessive deflections. This is, for example, documented by the data on the Děčín Bridge over the Labe in North Bohemia; see Fig. 9.

## Model B3 Improvement and Need for Inverse Analysis Many Bridges

Based on the parameter values obtained for Set 2 and on the comparisons with deflection measurements, it has been figured out that the multi-decade deflection prediction could be improved by replacing the B3 formulas (Bažant and Baweja 1995, 2000) for  $q_3$  and  $q_4$  with the following:

$$q_3 = (w/c)^3 q_2, \quad q_4 = 0.4(a/c)^{-0.7} \quad (4)$$

in which  $w/c, a/c =$  water-cement and aggregate-cement ratios, by weight.

However, the data on one or several bridges do not suffice to overcome the extreme scarcity of multi-decade test data. (Bažant and Li 2008a). For optimal recalibration of the B3 prediction of material parameters from concrete composition and strength, it will be necessary to gather data on the deflections of many box girder bridges and then conduct inverse finite element creep analysis with optimization.

## Uncertainty of Deflection Predictions and Calculation of Confidence Limits

Creep and shrinkage are notorious for their relatively high random scatter. For this reason, it has been argued during the last two decades (Bažant and Kim 1989, 1991) that the design should be made not for the mean deflections, but for some suitable confidence limits such as 95% (Bažant and Liu 1985, Bažant et al. 2007). Adopting the Latin hypercube sampling of the input parameters (Bažant and Liu 1985, Bažant and Kim 1989), one can easily obtain such confidence limits by repeating the deterministic computer analysis of the bridge according to model B3 8-times, one run for each of 8 different randomly generated samples of 8 input parameters.

The range of the cumulative distribution of each random input variable (assumed to be Gaussian) is partitioned into  $N$  intervals of equal probability. The parameter values corresponding to the centroids of these intervals are selected according to randomly generated Latin hypercube tables (these tables can be freely downloaded from the ITI website, <http://iti.northwestern.edu/generator>, so that a bridge designer would not need to work with a random number generator at all). The values from the rows of these tables are then used as the input parameters for  $N$  deterministic computer runs of creep and shrinkage analysis.

By experience, it is sufficient to chose  $N = n =$  number of random input parameters (here  $N = n = 8$ ). One random input variable is the environmental relative humidity  $h$ , whose mean and coefficient of variation are estimated as 0.70 and 0.2 (or 70% and 20%). The others

are the material characteristics  $q_1, q_2, q_3, q_4, q_5, k_t$  and  $\epsilon_\infty$ , representing the parameters of model B3. According to model B3, the means of these parameters for the KB Bridge are assumed as  $q_1 = 0.188, q_2 = 1.04, q_3 = 0.262, q_4 = 0.14, q_5 = 1.97, k_t = 19.2$ , and  $\epsilon_\infty = 0.0013$ . The estimated coefficient of variation is 23% for creep parameters  $q_1, q_2, q_5$ , and 30% for  $q_3, q_4$  (these have a higher uncertainty as they relate to long-term creep, for which the data are scarce). For shrinkage parameters  $k_t$  and  $\epsilon_\infty$  (Bažant and Panula 1978, Bažant and Baweja 1995, 2000), it is 34%.

The responses from each deterministic computer run for model B3 (set 2), particularly the mid-span deflections at specified times, are collected in one histogram of 8 values, whose mean  $\bar{w}$  and coefficient of variation  $\omega_w$  are the desired statistics. Knowing these, and assuming the Gaussian (or normal) distribution, one can get the one-sided 95% confidence limit as  $w_{95} = \bar{w}(1 + 1.645\omega_w)$  (i.e., the limit that is exceeded with the probability of 5%; in other words, the limit would be exceeded by one out of 20 identical bridges, which seems to give optimal balance between risk and cost).

The curves of the mean, and of the one-sided 95% and 5% confidence limit for the KB Bridge in Palau, are shown (for model B3, set 2) in Fig. 10. Note that the curves of the present finite element calculations according to the ACI and CEB models lie way outside the statistical confidence band obtained with model B3 (and the traditional prediction lies even farther).

Using the database (Bažant and Li 2008a) as the prior information, one could further improve the statistics of long-term deflection by means of Bayesian statistical analysis (Křístek and Bažant 1987).

The probabilistic problem of deflections is fortunately much easier than the problem of structural safety. For the latter, the extreme value statistical theory must be used since the tolerable probability of failure is  $< 10^{-6}$ , far less than the value of 0.05 that is acceptable for deflections.

## Summary of the Main Causes of Underestimation of Deflections and Prestress Loss

In the order of decreasing importance, the main causes are as follows:

1. Poor material model for creep and shrinkage.
2. Beam-type analysis instead of a full three-dimensional analysis.
3. Differences in the rates of shrinkage and drying creep due to different thicknesses of slabs in the box cross section.
4. Lack of statistical estimation of the range of possible responses.

Detailed conclusions will be presented in Part II.

## Appendix I: Resolution of 3rd Structural Engineers World Congress

1. *The structural engineers gathered at their 3rd World Congress deplore the fact the technical data on the collapses of various large structures, including the Koror-Babeldaob Bridge in Palau, have been sealed as a result of legal litigation.*
2. *They believe that the release of all such data would likely lead to progress in structural engineering and possibly prevent further collapses of large concrete structures.*
3. *In the name of engineering ethics, they call for the immediate release of all such data.*<sup>4</sup>

---

<sup>4</sup>Proposed at the congress by Z.P. Bažant, in the name of the following group of experts whose support has been obtained in advance: C. Andrade (Madrid), L. Belarbi (Missouri), N. Bićanić (Glasgow), I. Carol (Barcelona), L. Cedolin (Politecnico di Milano), T.-P. Chang (Taipei), J.-C. Chern (Taipei), W. Dilger (U. of Calgary), L. Elfgren (Lulea), R. Eligehausen (Stuttgart U.), E. Fairbairn (Rio de Janeiro), D.M. Frangopol (Lehigh), P. Gambarova (Politecnico di Milano), W. Gerstle (U. of New Mexico), N.M. Hawkins (Seattle), A.

## References

- [1] ABAM Engineers Inc. (1993). *Koror-Babeldaob bridge repairs: Basis for design*. Report submitted to Bureau of Public Workds, Koror, Republic of Palau, October, 1993.
- [2] ACI Committee 209 (1971) “Prediction of creep, shrinkage and temperature effects in concrete structures.”. *Designing for Effects of Creep, Shrinkage and Temperature in Concrete Structures, ACI-SP27*, Am. Concrete Institute, Detroit, pp. 51–93.
- [3] ACI Committee 209 (2008). *Guide for Modeling and Calculating Shrinkage and Creep in Hardened Concrete* ACI Report 209.2R-08, Farmington Hills.
- [4] ACI Committee 318 (2008). *Building code requirements for structural concrete (ACI 318-05) and commentary (ACI 318-05)*, American Concrete Institute, Farmington Hills.
- [5] Bažant, Z.P. (2000) “Criteria for rational prediction of creep and shrinkage of concrete” *Adam Neville Symposium: Creep and Shrinkage—Structural Design Effects*, ACI SP–194, A. Al-Manaseer, ed., Am. Concrete Institute, Farmington Hills, Michigan, 237-260.
- [6] Bažant, Z.P. (2001). “Creep of concrete” *Encyclopedia of Materials: Science and Technology*, K.H.J. Buschow et al., eds. Elsevier, Amsterdam, Vol. 2C, 1797–1800.
- [7] Bažant, Z.P. and Baweja, S. (1995). “Creep and shrinkage prediction model for analysis and design of concrete structures: ModelB3” *Materials and Structures* 28, pp. 357–367.
- [8] Bažant, Z.P. and Baweja, S. (2000). “Creep and shrinkage prediction model for analysis and design of concrete structures: Model B3.” *Adam Neville Symposium: Creep and Shrinkage—Structural Design Effects*, ACI SP–194, A. Al-Manaseer, ed., pp. 1–83 (update of RILEM Recommendation published in *Materials and Structures* Vol. 28, 1995, pp. 357–365, 415–430, and 488–495).
- [9] Bažant, Z.P., Hauggaard, A.B., Baweja, S. and Ulm, F.-J. (1997). “Microprestress-solidification theory for concrete creep. I. Aging and drying effects” *Journal of Engineering Mechanics, ASCE*, 123(11), pp. 1188–1194.
- [10] Bažant, Z.P., and Kim, Joong-Koo (1989). “Segmental box girder: Deflection probability and Bayesian updating.” *Journal of Structural Engineering* ASCE, 115 (10) 2528–2547.
- [11] Bažant, Z.P., and Kim, Joong-Koo (1991). “Segmental box girder: Effect of spatial random variability of material on deflections.” *J. of Structural Engineering* ASCE 117 (8), 2542–2547.
- [12] Bažant, Z.P., Kim, Joong-Koo, and Panula, L. (1991). “Improved prediction model for time-dependent deformations of concrete:” *Materials and Structures* (RILEM, Paris), Parts 1–2, Vol. 24 (1991), pp. 327–345, 409–421, Parts 3–6, Vol. 25 (1992), pp. 21–28, 84–94, 163–169, 219–223.
- [13] Bažant, Z.P., Křístek, V., and Vítek, J.L. (1992). “Drying and cracking effects in box-girder bridge segment.” *ASCE J. of Structural Engineering* 118 (1), 305–321.
- [14] Bažant, Z.P., and Li, Guang-Hua (2008a). “Comprehensive database on concrete creep and shrinkage.” *ACI Materials Journal* 106 (6, Nov.-Dec.), 635–638.
- [15] Bažant, Z.P., and Li, Guang-Hua (2008b). “Unbiased statistical comparison of creep and shrinkage prediction models”. *ACI Materials Journal* 106 (6, Nov.-Dec.), 610–621.
- [16] Bažant, Z.P., and Li, G.-H., Yu, Q., Klein, G., and Křístek, V. (2008) “Explanation of excessive long-time deflections of collapsed record-span box girder bridge in Palau”, *Prelim. Structural Engrg. Report 08-09/A222e*, Infrastructure Technology Institute (ITI), Northwestern University (presented at CONCREEP-8, Ise-Shima, Japan, Sept. 2008).

---

Ingraffea (Cornell University), M. Jirásek (CTU Prague), J.W. Ju (Los Angeles), M.T. Kazemi (Tehran), J.-K. Kim (KAUST, Korea), V. Křístek (CTU Prague), C. Leung (HKUST, Hong Kong), Z.-J. Li (Hong-Kong), K. Maekawa (U. of Tokyo), G. Maier (Politecnico di Milano), C. Majorana (U. of Padua), H. Mang (Vienna), P. Marti (ETHZ), H. Mihashi (Sendai), D. Novák (BTU Brno), J. Ožbolt (Stuttgart U.), B. Raghun-Prasad (Bangalore), I. Robertson (Honolulu), J.G. Rots (Delft), V. Saouma (Boulder), B. Schrefler (Padua), Susanto Teng (Singapore), S. Teng (Singapore), T. Tanabe (Nagoya), T. Tsubaki (Yokohama), F.-J. Ulm (MIT), J. van Mier (ETHZ), C. Videla (Santiago), M. Vořechovský (BTU Brno), K. Willam (UC Boulder), Y. Xi (Boulder), A. Zingoni (Cape Town).

- [17] Bažant, Z.P., Li, G.-H., and Yu, Q. (2008). “Prediction of creep and shrinkage and their effects in concrete structures: Critical appraisal.” *Creep, Shrinkage and Durability Mechanics of Concrete and Concrete Structures* (Proc., 8th Int. Conf. – CONCREEP-8, held in Ise-Shima, Japan), T. Tanabe et al. eds., CRC Press/Balkema, Taylor & Francis Group, Boca Raton–London, pp. 1275–1289.
- [18] Bažant, Z.P. and Liu, K.-L. (1985). “Random creep and shrinkage in structures: Sampling” *J. of Structural Engrg. ASCE* 111, pp. 1113–1134.
- [19] Bažant, Z.P. and Panula, L. (1978-1979). “Practical prediction of time-dependent deformations of concrete” *Materials and Structures* (RILEM, Paris): Part I, “Shrinkage” Vol. 11, 1978, pp. 307–316; Part II, “Basic creep” Vol. 11, 1978, pp. 317–328; Part III, “Drying creep” Vol. 11, 1978, pp. 415–424; Part IV, “Temperature effect on basic creep” Vol. 11, 1978, pp. 424–434.
- [20] Bažant, Z.P. and Prasannan, S. (1988). “Solidification theory for aging creep” *Cement and Concrete Research*, 18(6), pp. 923–932.
- [21] Bažant, Z.P. and Prasannan, S. (1989a). “Solidification theory for concrete creep: I. Formulation” *Journal of Engineering Mechanics ASCE*, 115(8), pp. 1691–1703.
- [22] Bažant, Z.P. and Prasannan, S. (1989b). “Solidification theory for concrete creep: II. Verification and application” *Journal of Engineering Mechanics ASCE*, 115(8), pp. 1704–1725.
- [23] Bažant, Z.P., and Yu, Q. (2006), “Reliability, brittleness and fringe formulas in concrete design codes”, *J. of Structural Engrg. ASCE* 132 (1), 3–12.
- [24] Bažant, Z.P., Yu, Q., Li, G.-H., Klein, G., and Krístek, V. (2010). “Excessive Deflections of Record-Span Prestressed Box Girder: Lessons learned from the collapse of the Koror-Babeldaob Bridge in Palau.” *ACI Concrete International* 32 (6), June, pp. 44–52.
- [25] Berger/ABAM Engineers Inc. (1995a). *Koror-Babeldaob Bridge modifications and repairs*, October 1995.
- [26] Berger/ABAM Engineers Inc. (1995b). *Koror-Babeldaob Bridge Repaire Project Report on Evaluation of VECP*, presented by Black Construction Corporation, June, 1995.
- [27] Brooks, J.J. (1984). “Accuracy of estimating long-term strains in concrete.” *Magazine of Concrete Research*, 36(128), 131–145.
- [28] Brooks, J.J. (2005). “30-year creep and shrinkage of concrete.” *Magazine of Concrete Research*, 57(9), 545–556.
- [29] Burgoyne, C. and Scantlebury, R. (2006). “Why did Palau bridge collapse?” *The Structural Engineer*, pp. 30-37.
- [30] Comité européen du béton (CEB) (1972) *Recommandations Internationales pour le Calcut et L'exécution des Ouvrages en Béton*, Paris, France.
- [31] DRC Consultants INC. (1996). *Koror-Babelthuap Bridge: Force Distribution in Bar Tendons*, February, 1996.
- [32] fib (1999). *Structural Concrete: Textbook on Behaviour, Design and Performance, Updated Knowledge of the of the CEB/FIP Model Code 1990*. Bulletin No. 2, Fédération internationale du béton (fib), Lausanne, Vol. 1, pp. 35–52.
- [33] Gardner, N.J. (2000). “Design provisions of shrinkage and creep of concrete” *Adam Neville Symposium: Creep and Shrinkage - Structural Design Effect* ACI SP-194, A. AlManaseer, eds., pp. 101–104.
- [34] Gardner N.J. and Lockman M.J. (2001). “Design provisions for drying shrinkage and creep of normal strength” *ACI Materials Journal* 98 (2), Mar.-Apr., pp.159–167.
- [35] Japan International Cooperation Agency (1990). *Present Condition Survey of the Koror-Babelthuap Bridge*, February, 1990.
- [36] Jirásek, M. and Bažant, Z.P. (2002). *Inelastic analysis of structures*, John Wiley & Sons, London and New York.

- [37] JSCE (1991). *Standard Specification for Design and Construction of Concrete Structure*, Japan Society of Civil Engineers (JSCE), in Japanese.
- [38] Křístek, V., and Bažant, Z.P. (1987). “Shear lag effect and uncertainty in concrete box girder creep.” *J. of Structural Engrg.*, ASCE 113 (3), 557–574.
- [39] Křístek, V., Bažant, Z.P., Zich, M., and Kohoutková, A. (2005). “Why is the initial trend of deflections of box girder bridges deceptive?” *Creep, Shrinkage and Durability of Concrete and Concrete Structures* (Proc., 7th Int. Conf.—CONCREEP 7, held in Nantes, France), G. Pijaudier-Cabot, B. Gérard and P. Acker, eds., Hermes Science Publishing, London, pp. 293–298.
- [40] Křístek, V., Bažant, Z.P., Zich, M., and Kohoutková (2006). “Box girder deflections: Why is the initial trend deceptive?” *Concrete International*, ACI, 28 (1), 55–63.
- [41] Křístek, V., Vráblík, L., Bažant, Z.P., Li, G.-H., and Yu, Q. (2008). “Misprediction of long-time deflections of prestressed box girders: Causes, remedies and tendon lay-out effect.” *Creep, Shrinkage and Durability Mechanics of Concrete and Concrete Structures* (Proc., 8th Int. Conf. – CONCREEP-8, held in Ise-Shima, Japan), T. Tanabe et al. eds., CRC Press/Balkema, Taylor & Francis Group, Boca Raton–London, pp. 1291–1295.
- [42] McDonald, B., Saraf, V., and Ross, B. (2003). “A spectacular collapse: The Koro-Babeldaob (Palau) balanced cantilever prestressed, post-tensioned bridge” *The Indian Constrete Journal* Vol. 77, No.3, March 2003, pp. 955–962.
- [43] Nilson, A.H. (1987). *Design of Prestressed Concrete*, 2nd edition, John Wiley & Sons, New York.
- [44] Parker, D. (1996). “Tropical Overload”, *New Civil Engineer*, December 5, 1996.
- [45] Pilz, M. (1997). *The collapse of the KB bridge in 1996*, Dissertation, Imperial College London.
- [46] Pilz, M. (1999). “Untersuchungenzum Einsturzder KB Brücke in Palau”, *Beton- und Stahlbetonbau*, May 1999, 94/5.
- [47] Shawwaf, Khaled (Dir., Dywidag Systems International USA, Bollingbrook, Illinois; former structural analyst on KB bridge design team), *Private communication*, September 18, 2008, Chicago.
- [48] SSFM Engineers, Inc. (1996) *Preliminary Assessment of Korrer-Babeldaob Bridge Failure*, prepared for US Army Corps of Engineers, October 2, 1996.
- [49] Troxell, G.E., Raphael, J.E. and Davis, R.W. (1958). “Long-time creep and shrinkage tests of plain and reinforced concrete” *Proc. ASTM* 58 pp. 1101-1120.
- [50] T.Y.Lin International (1996). *Collapse of the Koror-Babelthuap Bridge, Report*, T.Y.Lin International, October, 1996, pp.32.
- [51] Yee, A.A. (1979). “Record span box girder bridge connects Pacific islands” *Concrete International* 1 (June), pp. 22–25.

## List of Figures

1	(a) Koror-Babeldaob Bridge in Palau when built in 1977, (b) Babeldaob side after the collapse in 1996. . . . .	14
2	3D model of one half of the bridge and the cross sections of box girder at main pier and mid-span of main span. . . . .	14
3	Model B3 curve for adjusted $q_3$ and $q_4$ compared with the creep tests by Brooks (1984, 2005). . . . .	14
4	Mean deflections calculated by Model B3, ACI model, CEB model and GL model, in normal and logarithmic scales. . . . .	14
5	The same as Fig. 4 but for time extended up to 150 years, assuming that no retrofit and no collapse have taken place. . . . .	14

6	Deflections in normal and logarithmic scales, computed with model B3 for (1) no drying creep; (2) no shrinkage and no drying creep; (3) uniform creep and shrinkage over the cross section. . . . .	14
7	Prestress loss in tendons at main pier by Model B3, ACI model, CEB model and GL model in normal and logarithmic scales. . . . .	14
8	Excessive deflections observed in 4 Japanese bridges (JRA = Japan Road Association). . . . .	14
9	Excessive deflections observed in a continuous bridge in Czech Republic. . . . .	14
10	Mean response and 95% confidence limits of Model B3, in normal and logarithmic scales. . . . .	14

Table 1: Summary of strain relief tests of prestressed tendons of KB Bridge in Palau (Berger/ABAM 1995a)

Tendon	Location	$\Delta_1$ ( $\mu\epsilon$ )	$\Delta_2$ ( $\mu\epsilon$ )	$\Delta_3$ ( $\mu\epsilon$ )	Mean $\Delta$ ( $\mu\epsilon$ )	$\sigma$ (MPa)
1	1	1640	1640	1630	1637	327.3
	2	1650	1640	1650	1647	329.3
	3	1680	1700	1710	1697	339.3
	Average					332.0
2	4	1810	1820	1790	1807	361.3
	5	1810	1800	1790	1800	360.0
	6	1780	1790	1790	1787	357.3
	Average					359.6
3	7	2250	2230	2220	2233	446.7
	8	2220	2220	2210	2217	443.3
	9	2170	2150	2170	2163	432.7
	Average					440.9

a)



b)



Fig. 1

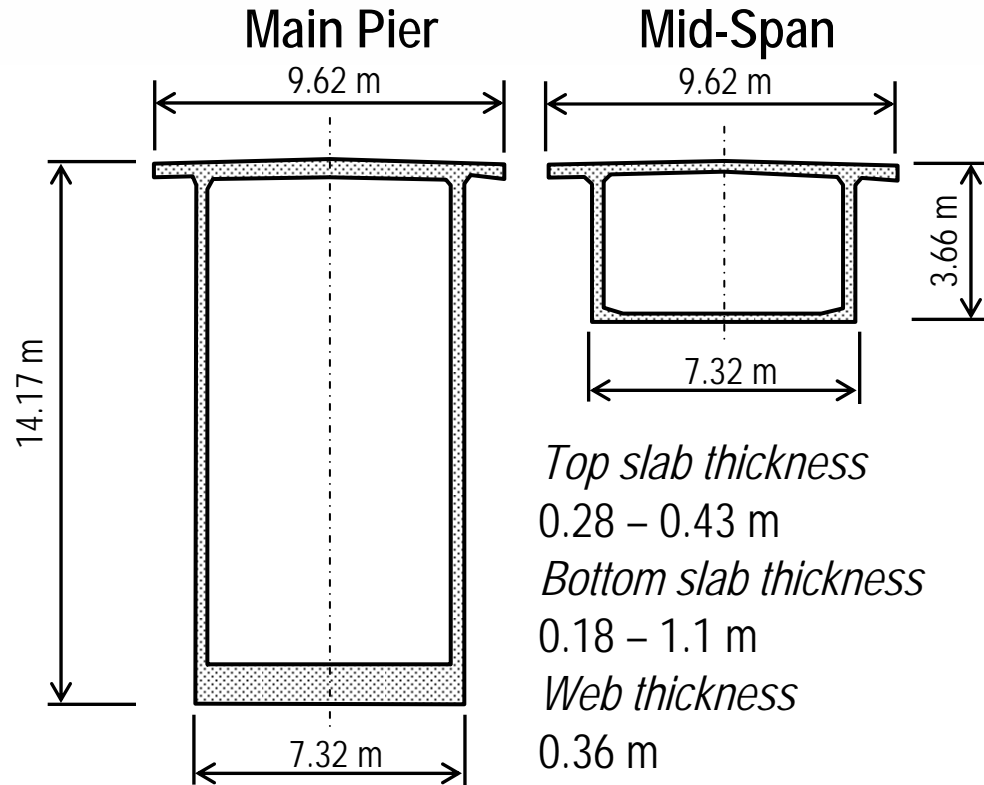
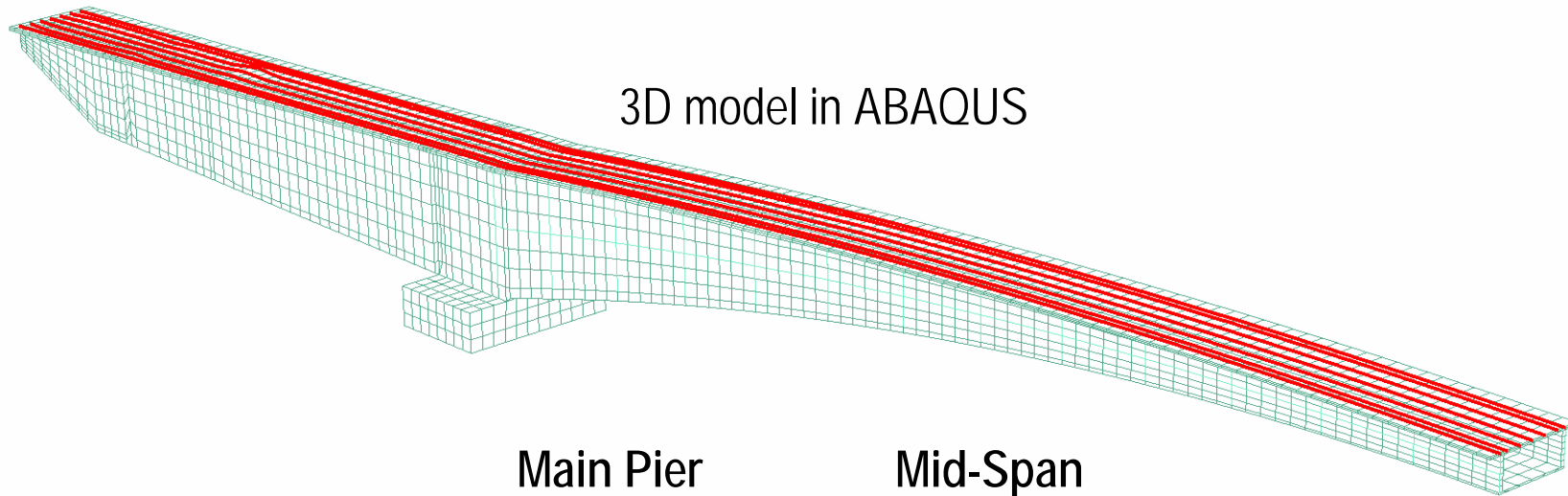


Fig. 2

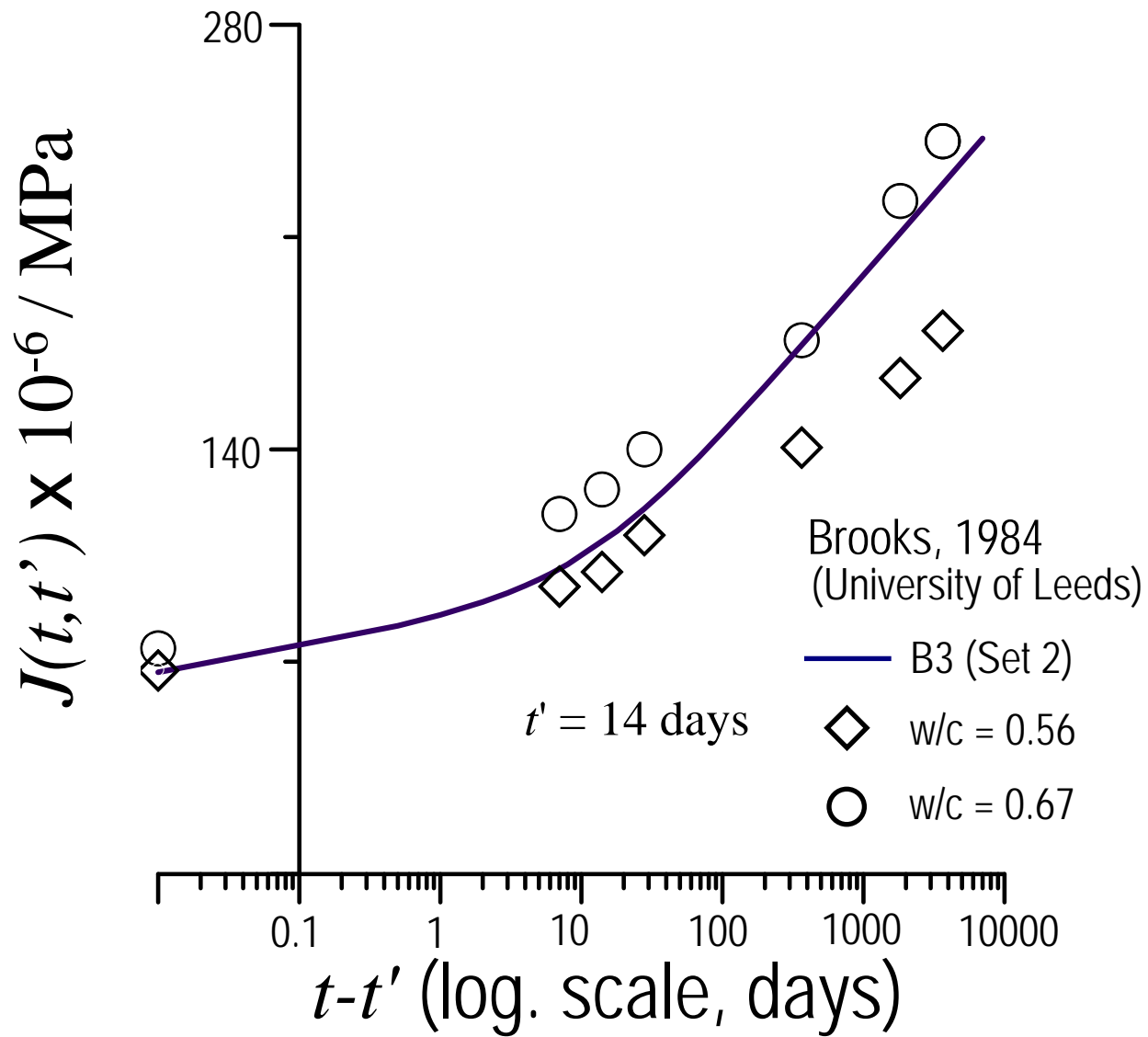


Fig. 3

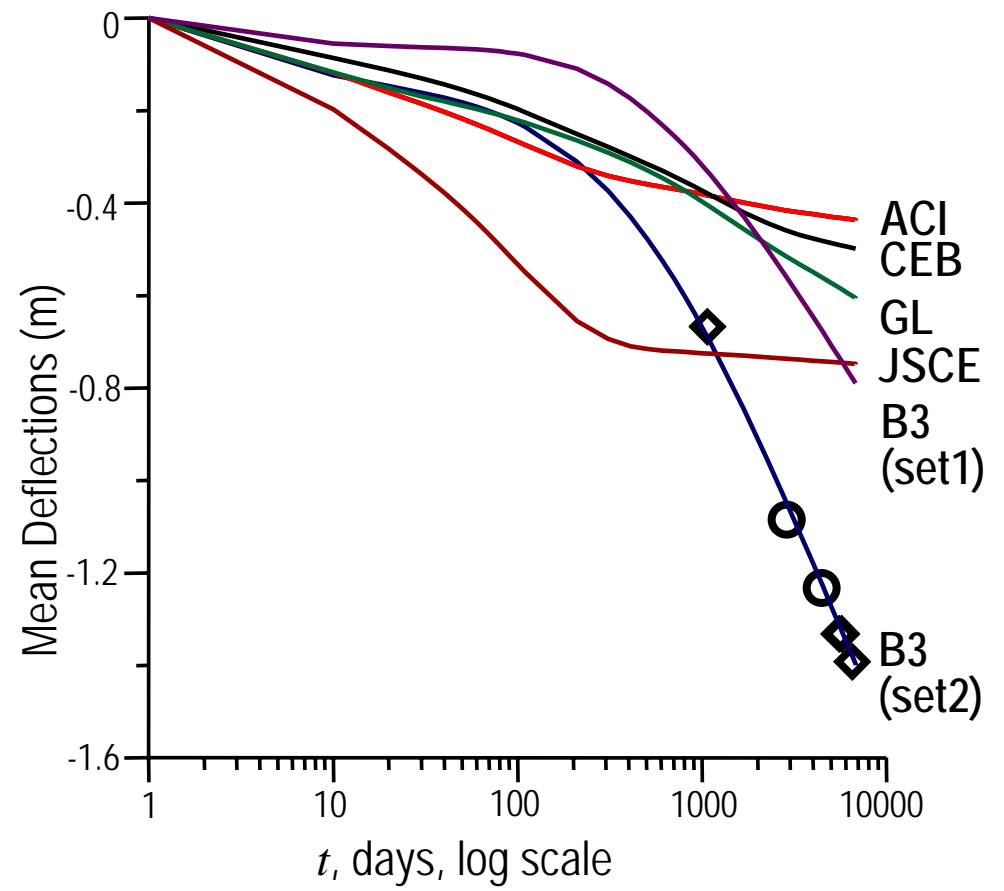
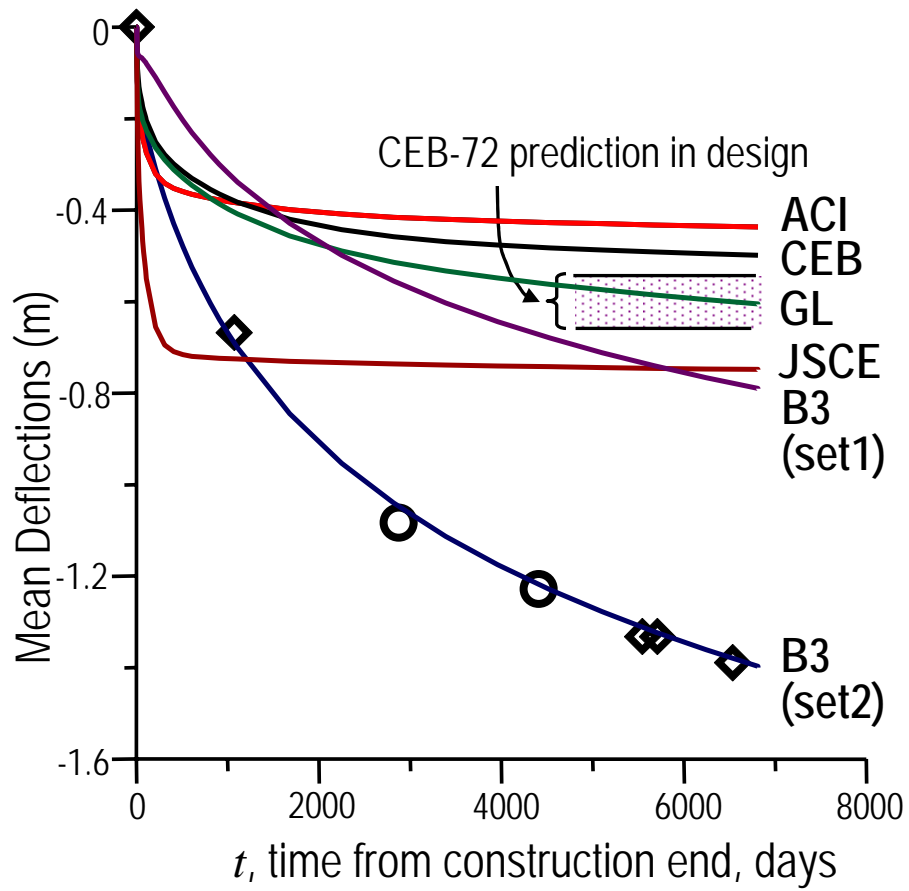


Fig. 4

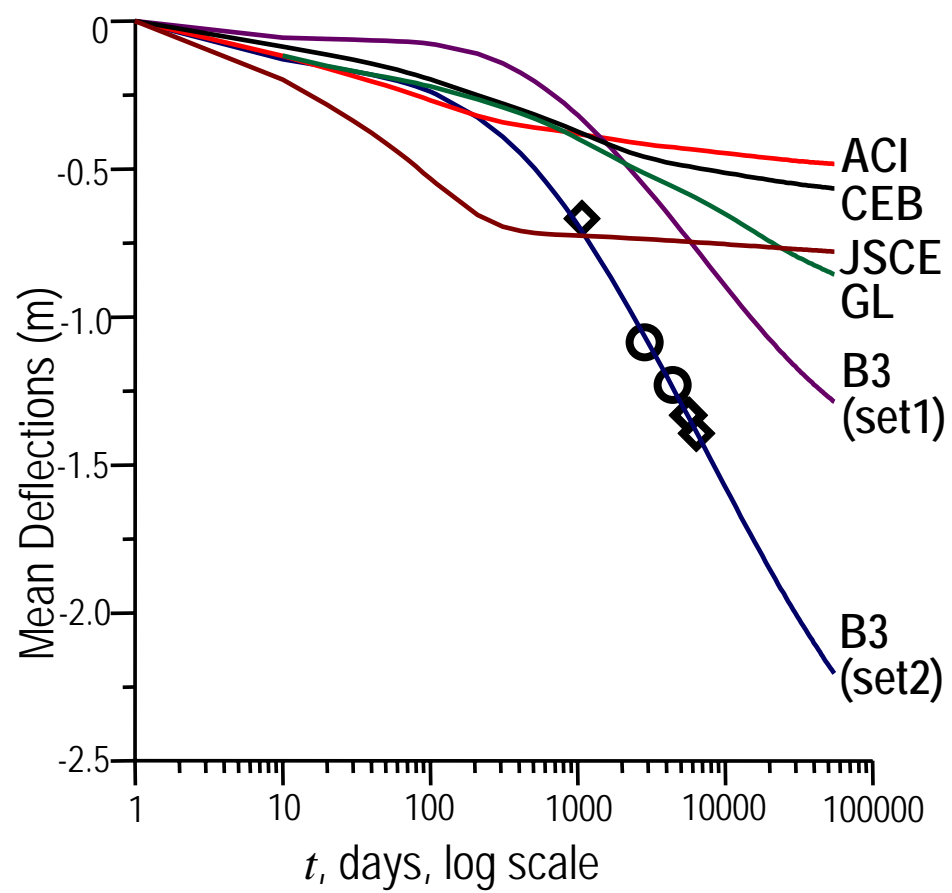
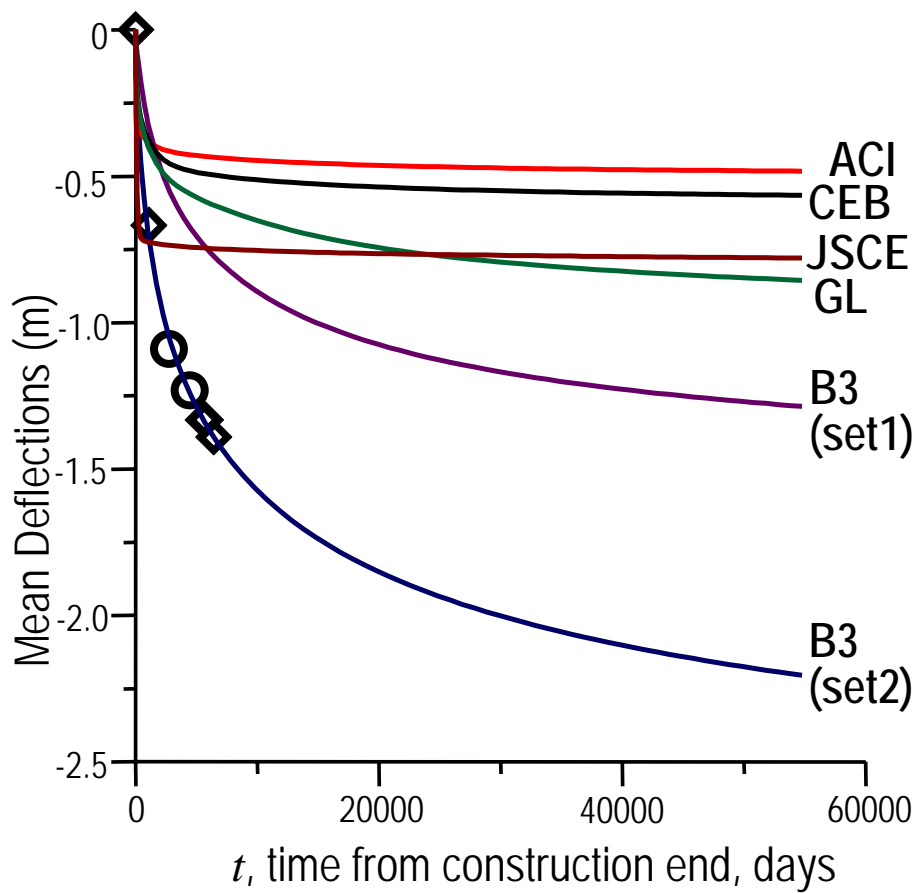


Fig. 5

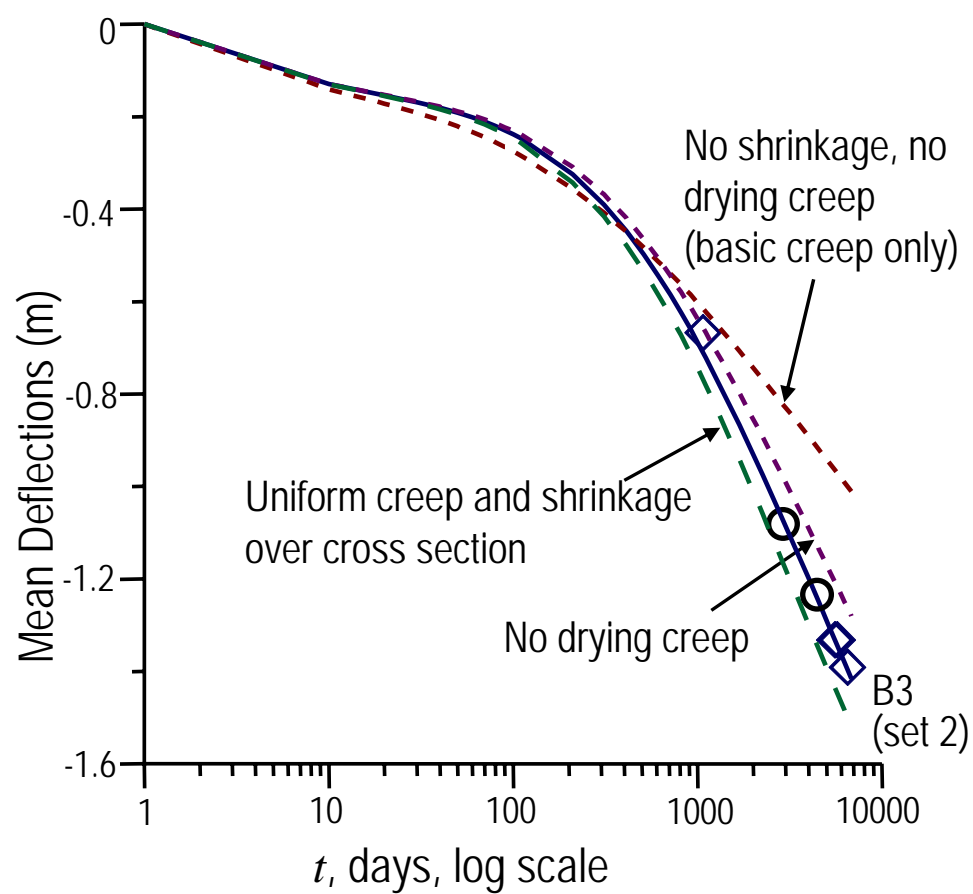
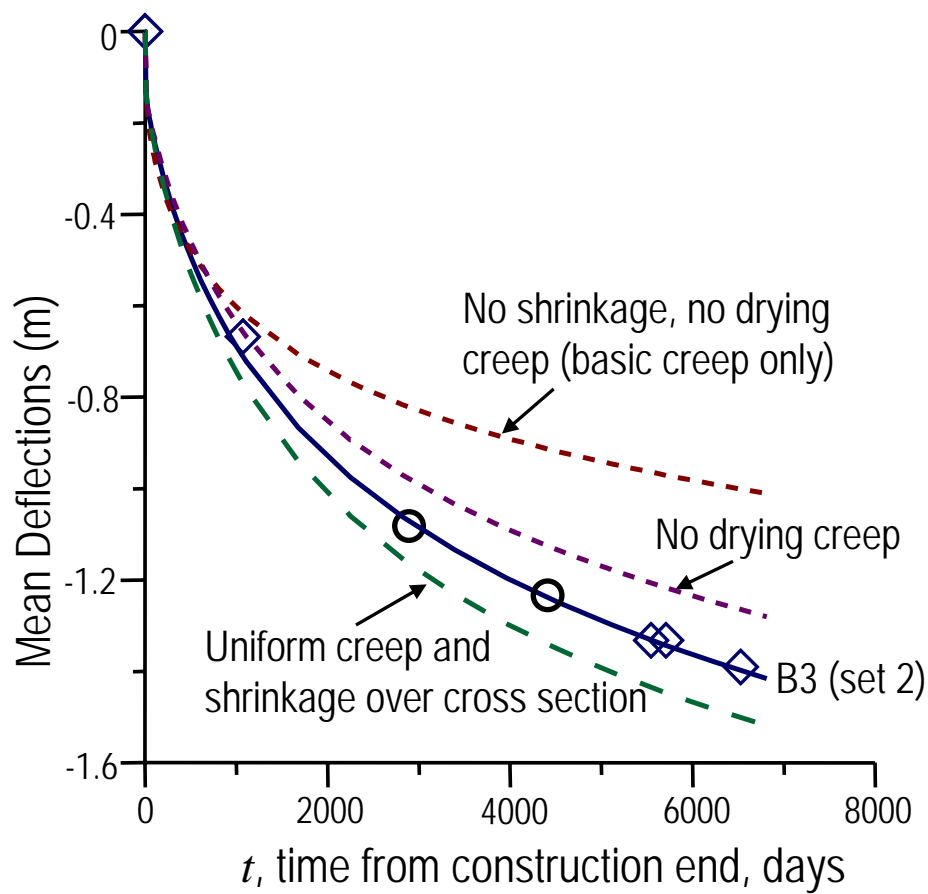


Fig. 6

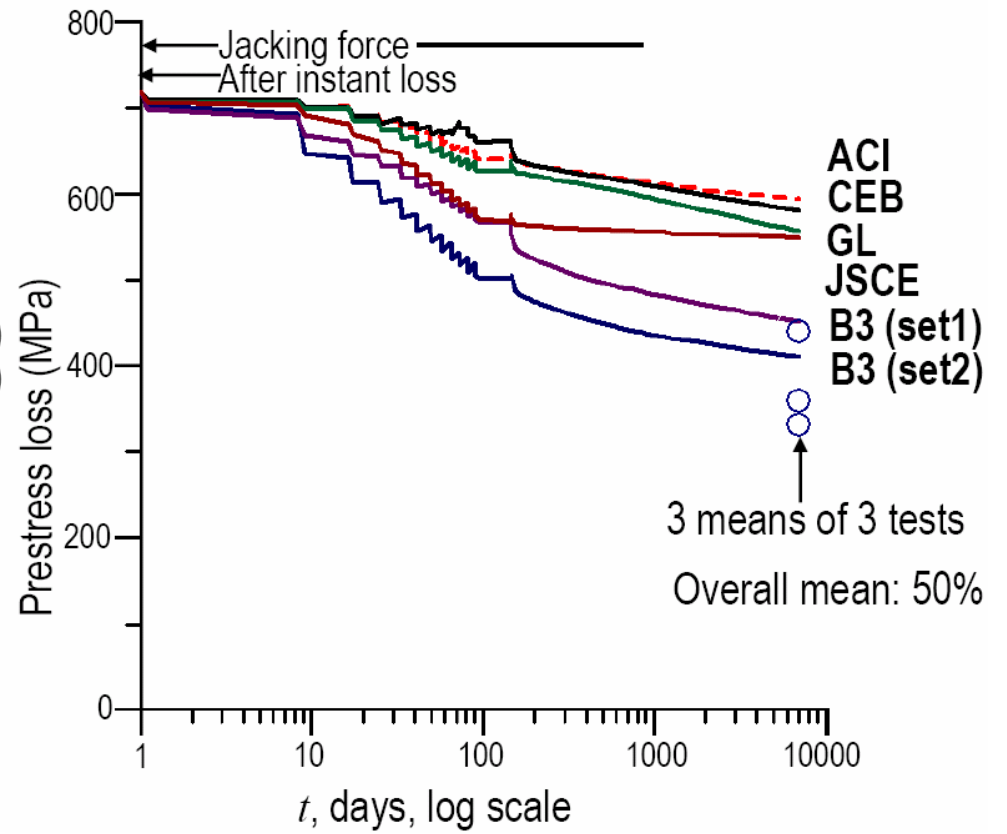
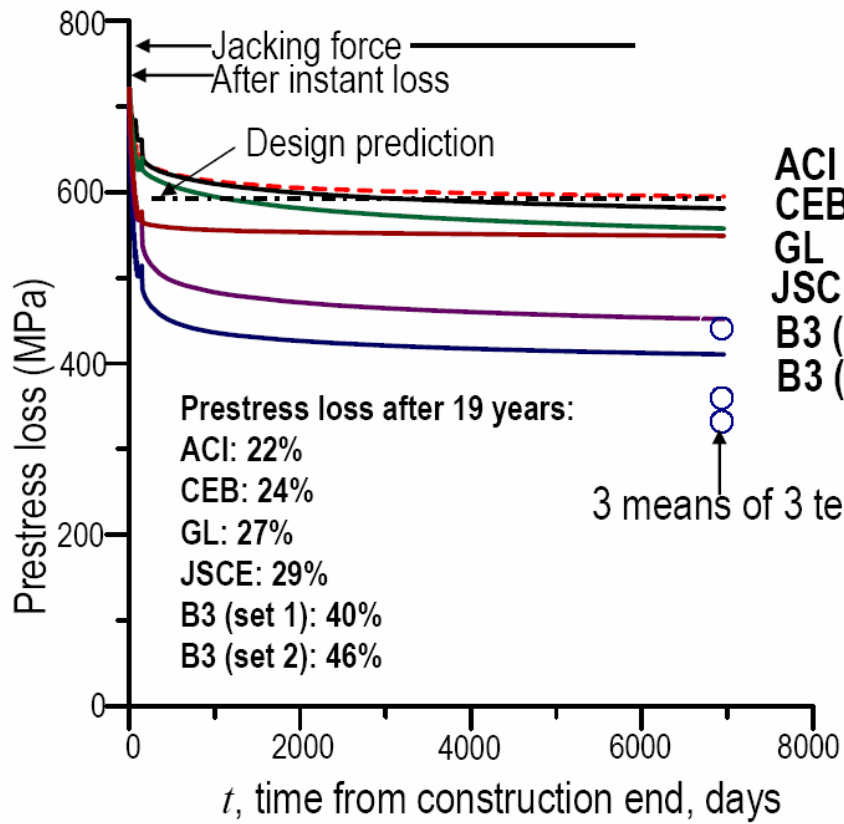


Fig. 7

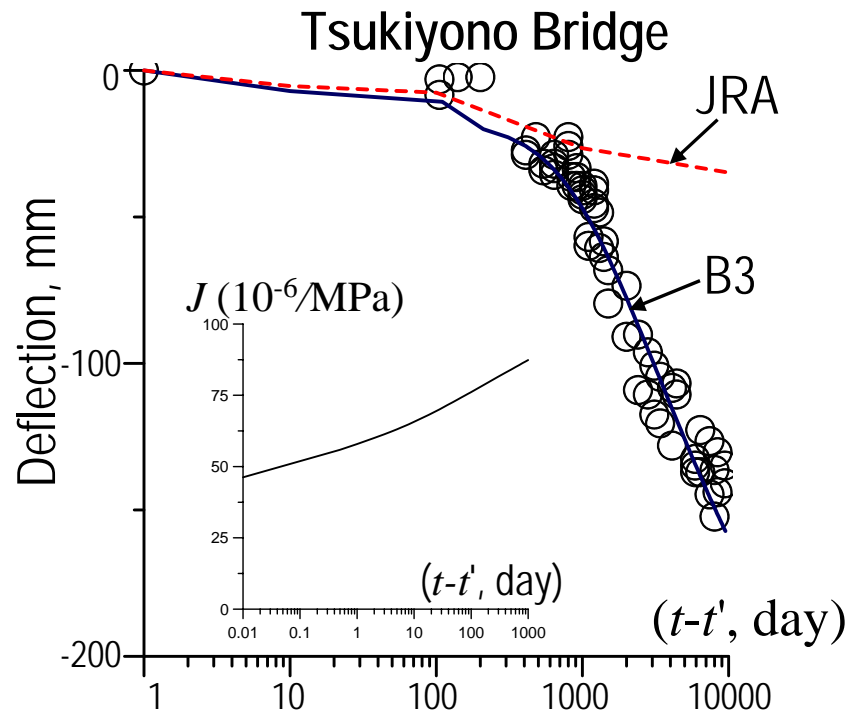
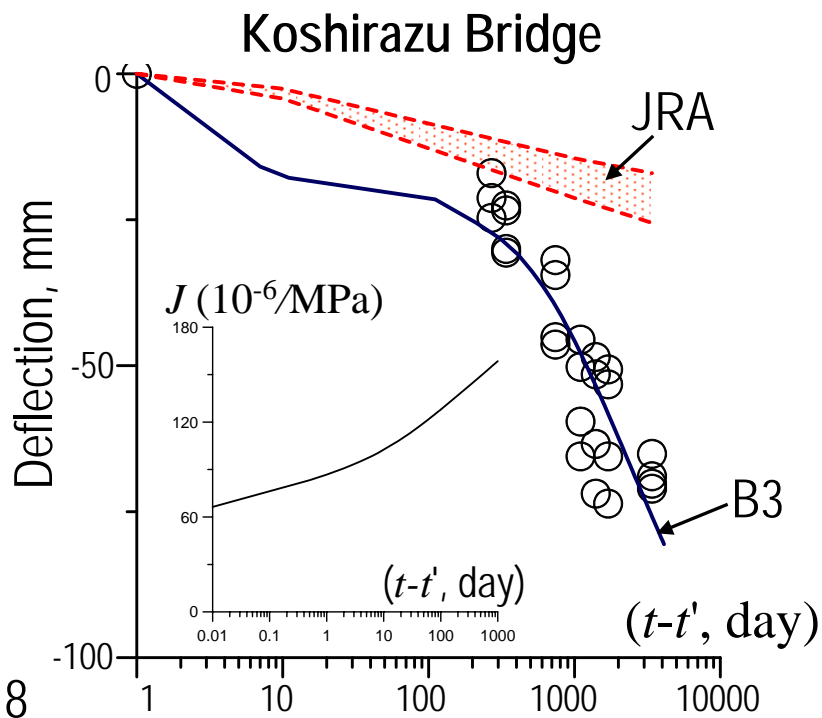
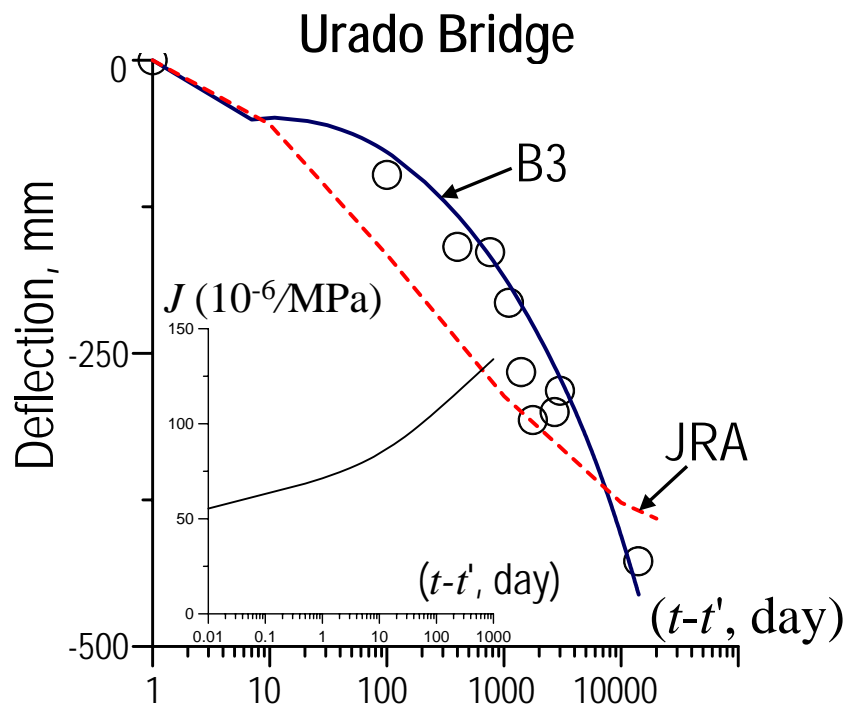
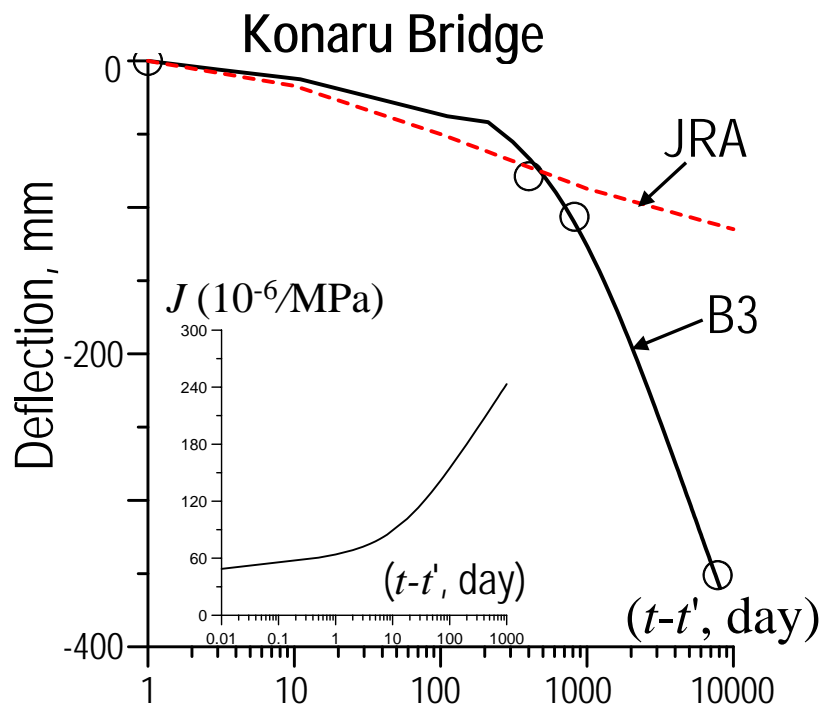


Fig. 8

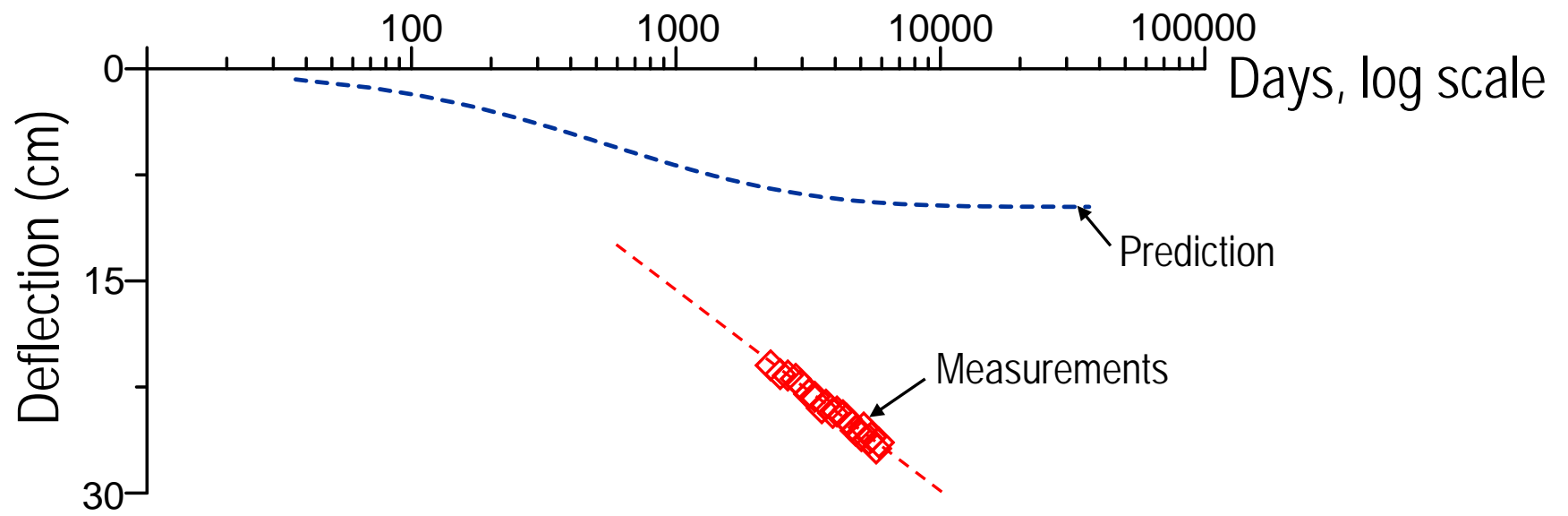


Fig. 9

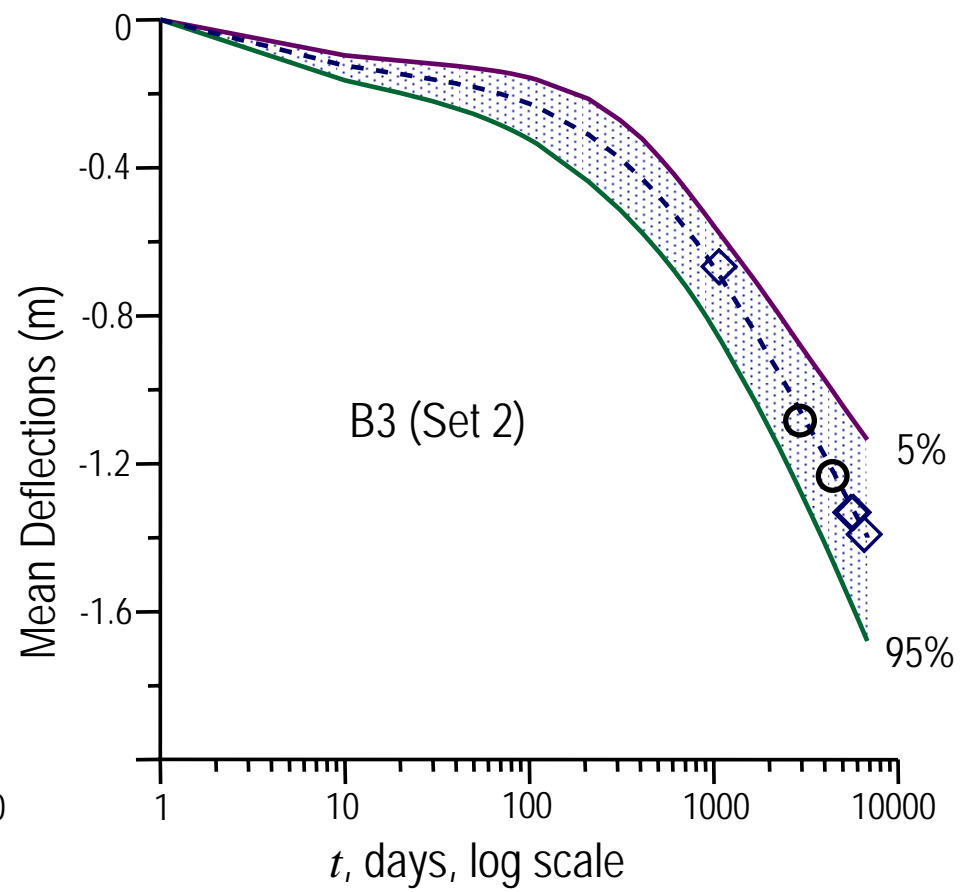
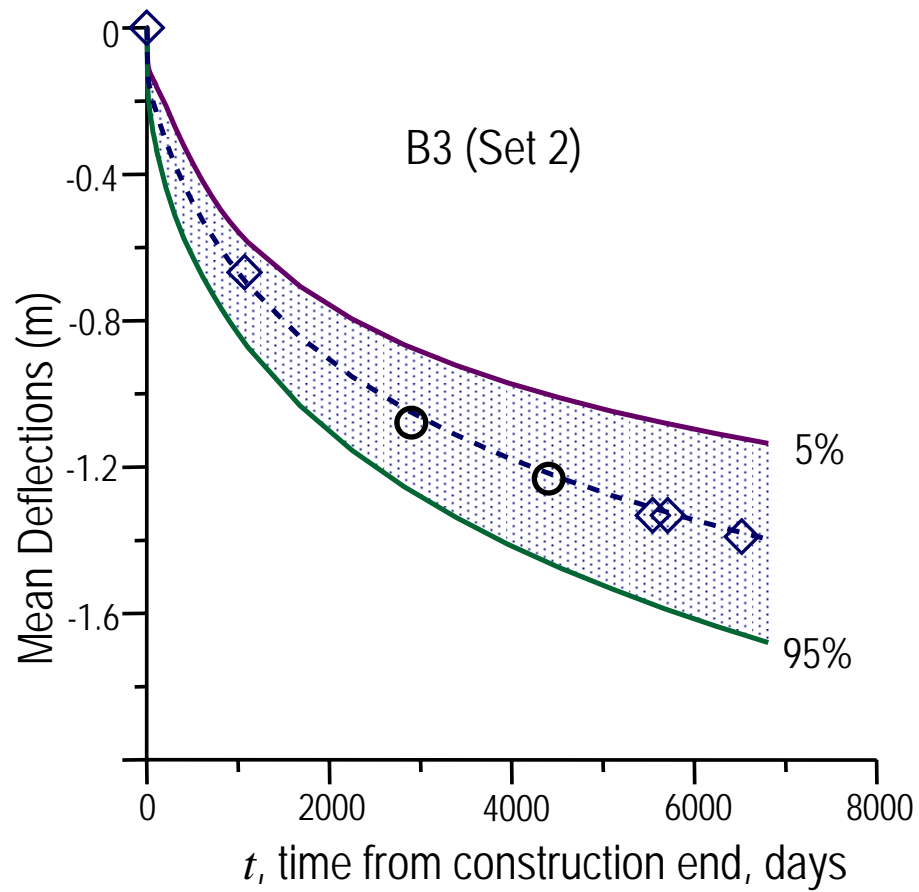


Fig. 10

# Excessive Long-Time Deflections of Prestressed Box Girders: II. Numerical Analysis and Lessons Learned

Zdeněk P. Bažant<sup>1</sup>, Qiang Yu<sup>2</sup> and Guang-Hua Li<sup>3</sup>

**Abstract:** As a sequel to part I, which clarified the causes of the unexpectedly large deflections of the Koror-Babeldaob (KB) Bridge in Palau, this part II presents the numerical procedure and reviews the lessons learned. The box girder represents a thick shell which is discretized by 8-node three-dimensional finite elements. Except for corrections due to cracking, concrete creep is assumed to follow aging linear viscoelasticity and is modeled by a rate-type law based on the Kelvin chain whose properties are adjusted for humidity conditions and temperature. In each time step and at each integration point, Widder's formula is used to convert the aging compliance function to a continuous retardation spectrum for the current age of concrete, and discretization of the spectrum yields the current elastic moduli of the Kelvin units. The shrinkage strains depend on the environmental humidity and the thickness of each plate in the cross section. The computations proceed according to Bažant's exponential algorithm which is unconditionally stable and reduces the problem to a sequence of elasticity problems with an orthotropic effective stiffness of material and non-isotropic inelastic strains, different for each integration point in each time step. These problems are solved by commercial software ABAQUS. The segmental construction sequence is also modeled. The computer results reported in Part I explain the excessive deflections and compare the performance of various material models for creep and shrinkage. Finally, the lessons learned are formulated and recommendations made.

## Introduction

The creep and shrinkage analysis of segmentally built prestressed concrete box girders is in practice often conducted in a rather simplified way. It usually relies on the material models recommended by ACI, CEB ('fib') and JSCE, which grossly underestimate multi-decade creep, give unrealistic shapes of creep and shrinkage curves and unrealistic effects of drying, and assume the creep to terminate at some fixed upper bound, for which no experimental support exists. In computer programs for long-time creep, the box girder is typically simplified as a beam with cross sections remaining plane, except that shear lag corrections for the effective width of top slab are usually made.

The analysis of the bridge in Palau confirms that such simplifications are unrealistic. However, as demonstrated by the computer results in Part I, a significant improvement is made possible by the advances in material modeling of creep and shrinkage. The computational approach, which is usable for all box girder bridges, will now be presented.

## Creep Structural Analysis Utilizing ABAQUS

By step-by-step analysis, the structural creep problem gets reduced to a sequence of elastic finite element analyses for an elastic stress-strain relation with inelastic strain, one analysis for each time step (which is an approach proposed in Bažant 1967). Each such analysis can be carried out with a commercial finite element program. So one merely needs to find a suitable

---

<sup>1</sup>McCormick Institute Professor and W.P. Murphy Professor of Civil Engineering and Materials Science, Northwestern University, 2145 Sheridan Road, CEE/A135, Evanston, Illinois 60208; z-bazant@northwestern.edu.

<sup>2</sup>Post-doctoral Research Associate, Northwestern University.

<sup>3</sup>Graduate Research Assistant, Northwestern University.

commercial finite element program which has the requisite geometric and material modeling features. The software ABAQUS (SIMULIA, Providence, Rhode Island) has been chosen.

The plates (slabs and walls) of the box girder are subdivided into 8-node isoparametric finite elements (Fig. 1). Except in the top slab, the finite elements are chosen to extend through the whole thickness since the stresses caused by load do not vary significantly through the thickness and plate bending is not important. Although, for drying creep and shrinkage, accurate modeling may generally require the wall thickness to be subdivided into at least six finite elements, model B3 makes it possible to avoid thickness subdivision because it is based on an analytical solution of drying according to the diffusion theory. This approach would not be accurate for cross sections subjected to flexure or highly eccentric compression, because the creep specimens in the underlying database are loaded centrally and are drying symmetrically. However, for the box girder, accuracy is good because the resultant of normal stresses across the wall is everywhere nearly centric, same as is standard creep tests.

In view of symmetry, only one half of the bridge is analyzed. Together with the pier, it is subdivided into 5036 hexahedral elements. The mesh, automatically generated by ABAQUS, is shown in Fig. 1. The prestressing tendons and the non-prestressed steel bars are subdivided into further 6764 bar elements connected rigidly (with no slip) to the nodes of the three-dimensional mesh (the information on unprestressed steel is found in ABAM 1993). Sufficiency of mesh fineness has been validated by checking that a finer mesh with 20144 hexahedral elements would yield only a negligible improvement of the computed elastic deflections.

The differences in the ages of various segments, the sequential prestressing at various times, and the step-wise load increase in the individual segments during construction (including the extra weight of 1068 kN, or 240 kips, introduced during the construction by the formwork carrying traveller) are taken into account according to the actual cantilever erection procedure. To simulate this segmental erection procedure, the elements are deactivated at first and then progressively reactivated according to the construction sequence (the ABAQUS keyword that enables this helpful feature is ‘*model change, remove/add*’).

The individual prestressing bars, the number of which is 316 above the main pier, were modeled as 2-node line elements, attached to concrete at the nodes. The individual bars of unprestressed steel reinforcement were modeled similarly. The introduction of prestress was handled in ABAQUS automatically by the keyword ‘*initial conditions, type=stress, user*’ in the keyword editor. So, it sufficed to specify the prestress values of every tendon in user subroutine *sigini* of ABAQUS. Although the tendons were not prestressed fully at one time (T.Y. Lin International 1996), each tendon was assumed to get fully prestressed 7 days after its anchoring segment had been cast. Capturing the time schedule accurately matters for the initial deflection history, but not for multi-year deflections.

Since the tendons are straight, the curvature friction is nil and only the wobble friction is modeled. To do that, the initial prestress is diminished according to the length of each individual tendon using the wobble coefficient  $\kappa = 0.0003$  /ft. or 0.00098/m (e.g., Nilson 1987, DRC 1996).

The prestress losses caused by creep and shrinkage, by sequential prestressing of tendons and by relaxation of steel stress  $\sigma_s$  are automatically reproduced by ABAQUS. For constant strain  $\epsilon$ , the relaxation is assumed to follow the CEB-FIP (1990) formula for prestress loss ratio:  $\rho = (\sigma_0 - \sigma_s)/\sigma_0 = \rho_{1000}(t/1000 \text{ hours})^k$  where  $\sigma_0$  = initial prestress,  $k \approx 0.12$  and  $\rho_{1000} \approx 6.5\%$ . Since  $\epsilon$  equals the strain in concrete, which varies with time  $t$ , this formula is generalized as

$$\Delta\sigma_s = E_s\Delta\epsilon - r(\sigma_0 - \sigma_s)^{1-1/k}\Delta t \quad (1)$$

where  $r = k(\sigma_0\rho_{1000})^{1/k}/(1000 \text{ hours})$ . This stress-strain relation for tendon steel in time step  $\Delta t$  is based on the Maxwell model for creep with stress-dependent viscosity and is implemented in user subroutine *uexpan* of ABAQUS. Check that, for  $\Delta\epsilon = 0$ , integration of Eq. (1) yields the CEB-FIP formula.

## Effects of Slab Thickness, Temperature and Cracking

Model B3 predicts separately the basic creep of the material (i.e., the part of creep unaffected by moisture content variation) and the additional effects of drying. These effects consist of the average shrinkage and average drying creep (or stress-induced shrinkage) in the cross section, and depend on the effective thickness  $D$  of the cross section.

The shrinkage is modeled by inelastic strain increments in user subroutine *uexpn*. In each of the 25 segments of the central half-span, the plate thicknesses  $D$  and concrete ages are different, resulting in a different shrinkage function and a different compliance function for each plate of each segment.

Recent research (Křístek et al. 2006) has revealed extreme sensitivity of box girder deflections to the differences in the rates of shrinkage and drying creep between the top and bottom slabs. Thanks to the fact that model B3 is physically based, the differences in its parameters between top and bottom can be assessed realistically, based on the known drying rates.

These rates are characterized by the shrinkage half-times, for which the diffusion theory gives the equation  $\tau_{sh} = k_t(k_s D)^2$  (see Eq. 1.11 in Bažant and Baweja 2000);  $k_s$  is a shape parameter (equal to 1 for plates), and  $k_t$  is a permeability parameter for which a crude empirical estimate exists;  $k_t = 0.03/C_1$  (see Eq. 28.12 in Jirásek and Bažant 2002) where  $C_1 = k_a P_1 =$  diffusivity,  $k_a \approx$  constant, and  $P_1 =$  permeability of concrete, which depends on temperature and the extent of cracking.

The mean temperature of the bottom slab and webs was probably 25 °C (77 °F), but the top slab with the roadway layer, exposed on top to intense tropical sunlight, was probably during the day some 20 °C (36 °F) warmer. According to the curves for the temperature effect on permeability in Fig. 10.3 (b,c) of Bažant and Kaplan 1996, this likely caused a 10-fold decrease of  $\tau_{sh}$  for the top slab. Furthermore, while no cracking could have occurred in the compressed bottom slab and webs, the top slab must have developed hairline cracks since it was under tension due to the excessive prestress loss. Based on the experiments reported (Bažant et al. 1987), cracks of width 0.15 mm will increase the drying rate about 3-times. The same may be assumed for the top slab, and so, according to Eq. 1.20 of Bažant and Baweja 2000, the value of  $k_t = 19.2$  is used for the bottom slab and the webs, and the value of  $k_t = 19.2/30 = 0.64$  for the top slab. In calculations of deflections, the stiffness of the pavement layer is entirely neglected since it is unreinforced and in tension. However, since the pavement tends to decelerate the drying rate of top slab, its effective thickness is taken into account in shrinkage modeling.

It used to be commonplace to consider one  $V/S$  value as a characteristic of the whole cross section, i.e., to take  $D = 2V/S$  with  $V =$  volume and  $S =$  surface of cross-section slice of the whole box. In that case,  $D$  was a property of the whole cross section, resulting in a supposedly uniform shrinkage and supposedly uniform creep properties. Recently, however, it has been shown (Křístek et al. 2006) that, to avoid serious errors (which usually lead to overoptimistic interpretation of small early deflections), differences in the drying rate due to different thicknesses  $D_i$  ( $i = 1, 2, 3$ ) of the top slab, the bottom slab and the webs must be taken into account.

A simple way to do that, demonstrated in Křístek et al. (2006), is to apply a model such as B3 separately to each plate of the cross section. Since the drying half-times are proportional to slab thickness square, the thickness differences then yield different shrinkage and different drying creep compliance in different plates.

According to models such as that of ACI, a thickness increase allegedly scales down the creep and shrinkage through a certain constant multiplicative factor, including the alleged final value for infinite time. However, in reality (except for a small multiplicative reduction due to a higher degree of hydration reached in thicker slabs), a thickness increase causes a delay, properly modeled as deceleration and characterized as an increase of the shrinkage half-time, which is proportional to the thickness square (e.g., if the ultimate shrinkage for a slab 0.10 m or 4 in. thick is reached in 10 years, for a slab 1 m or 40 in. thick it is reached in 1000 years, i.e., virtually never).

Because of excessive prestress loss, the top slab is found to get into tension after the first year. Although no large tensile cracks were observed (JICA 1990, ABAM 1993 reported sparse fine cracks in the first 6 segments from the mid-span). Calculations show that if the tensile strength limit  $f'_t$  is ignored, the tensile stresses in the top slab would in later years reach the stress of about  $2f'_t$  where  $f'_t$  = tensile strength, estimated as  $6 \text{ psi} \sqrt{f'_c/\text{psi}} = 3.0 \text{ MPa} = 433 \text{ psi}$ . The most realistic model would be the cohesive crack model with rate-dependent softening, applied to growing parallel cracks of uniform spacing, with the material between the cracks considered as viscoelastic (Bažant and Li 1997). However, to implement this model with ABAQUS has been found to be virtually impossible.

After trying with ABAQUS various simplifications, the computations were eventually run under the simplifying assumption that the effective incremental modulus  $E''$  for the current time step (which includes the effect of creep and is used in steps 2 and 3 of the Appendix) gets reduced to  $E''/4$  when the tensile stress exceeds  $0.7f'_t$  (Fig. 2). With this simplification, the maximum computed tensile stress in the top slab is about 3.0 MPa, and the corresponding strain is  $1.83\times$  larger than the actual strain at peak tensile stress. With hardening due to positive  $E''/4$  compensated by the 70% strength reduction, the tensile stress resultant happens to be about the same as that obtained with a more realistic model consisting of a bilinear softening stress-strain relation with an unreduced tensile strength limit and the softening modulus of about  $-E''/3$ . The error compared to this more realistic model is estimated as  $< 1\%$  of the deflection. For comparison, if unlimited tensile strength were assumed, the computed deflections would have been about 4% smaller.

Combined with the steel stiffness, the softening of concrete would have resulted in overall tension stiffening, which would have been easy to implement had all the computations been programmed. But in the algorithm with ABAQUS the tensile softening turned out to be intractable because it would have interfered with the programming of exponential algorithm for creep. This is why a positive modulus  $E''/4$  had to be adopted.

## Creep Analysis and Rate-Type Model Based on Kelvin Chain

The traditional characterization of concrete creep by the creep coefficient, giving the creep-to-elastic strain ratio, must be avoided (Bažant 1975, 1982, RILEM 1988, Bažant and Baweja 1995, Jirásek and Bažant 2002) because, due to pronounced short-time creep for durations  $> 0.0001$  second, the definition of elastic modulus is ambiguous. Significant errors have often been caused by combining the creep coefficient with an incompatible value of the conventional elastic modulus. Thus the analysis must properly be based on the compliance function  $J(t, t')$ , defined as the total strain  $\epsilon_{xx}$  at age  $t$  caused by a sustained uniaxial stress  $\sigma_{xx} = 1$  applied at age  $t'$ .

An individual material constitutive law corresponding to every different creep and shrinkage prediction model has been developed for the user subroutine *umat* of ABAQUS. The three-dimensional generalization is obtained under the assumption of material isotropy and a time-independent Poisson ratio  $\nu$  (Bažant 1975, 1982, RILEM 1988 ;  $\nu = 0.21$  is used here, based on core sample tests, Berger/ABAM 1995). Linear viscoelasticity implies the principle of superposition in time, whose direct application gives the stress-strain relation in the form of a history integral. However, major deviations from the principle of superposition are caused by tensile cracking and by time variations of humidity and temperature (and also by triaxial damage in compression which, however, can be ignored for service states). Therefore, the history integrals are inapplicable and the corrections for cracking, etc., must be introduced after converting the compliance function to an equivalent rate-type creep law, which is here based on the Kelvin chain model. This conversion also greatly improves computational efficiency.

In the case of model B3, conversion of the compliance function of basic creep to a rate-type creep law is particularly easy. It can be done according to the solidification theory (Bažant and Prasanna 1988, 1989a,b, Jirásek and Bažant 2002), in which the aging is taken into

account by means of volume growth of the solidifying component, and by a gradual increase with age of the flow term viscosity. Thus it is possible to use a non-aging compliance function for the solidifying component, for which one can uniquely determine a continuous retardation spectrum. This spectrum can be readily obtained from Widder's formula (Tschoegl 1989), a simple explicit formula which is based on the inversion of Laplace transform (Bažant and Xi 1995). The parameters of the Kelvin chain model are in this case constant (i.e., non-aging) and are simply obtained as a discrete representation of the continuous spectrum.

For empirical models such as those of ACI, CEB, JSCE and GL, such an approach is impossible since a non-aging constituent in the sense of the solidification theory cannot be identified for these models. Therefore, compliance curves that change with the age at loading must be used, as defined by  $J(t, t')$ . This problem was handled in the 1970s by considering the retardation (or relaxation) spectrum to be age dependent, which caused that the spectrum of elastic moduli  $E_\mu(t)$  ( $\mu = 1, 2, 3, \dots$ ) of the Kelvin (or Maxwell) chain model had to be considered as age-dependent, too (Bažant 1975, 1982, RILEM 1988). Unfortunately, the least-square identification of these moduli as functions of age appeared to be an ill-conditioned problem (since different functions  $E_\mu(t)$  provided almost equally good fits of  $J(t, t')$ , even if they were not increasing monotonically as required by aging).

An age-independent spectrum can nevertheless be used within each sufficiently short time step, such that the creep properties, including the moduli and viscosities of the Kelvin chain model, could be considered to be approximately age independent, corresponding to concrete age  $t_{n-1/2}$  in the middle of the time step. Indeed, for the stress changes within a short enough time step, the concrete may be considered to behave as a non-aging linearly viscoelastic material characterized by the Kelvin chain moduli and viscosities corresponding to age  $t_{n-1/2}$ , which depend only on the compliance curve  $J_{n-1/2}(t) = J(t, t_{n-1/2})$ . This curve corresponds to one retardation spectrum and is approximated by one Kelvin chain, having constant moduli  $E_\mu(t_{n-1/2})$  ( $\mu = 1, 2, 3, \dots$ ), applicable to the current time step only.

For the average age  $t_{n-1/2}$  corresponding to every time step, the compliance curve  $J_{n-1/2}(t)$  corresponding, e.g., to the ACI, CEB or GL model, one must identify the corresponding retardation spectrum corresponding to age  $t_{n-1/2}$ . This can be done according to Widder's explicit formula (Bažant and Xi 1995), before starting the step-by-step finite element analysis of the structure. This continuous retardation spectrum is approximated by a set of discrete spectral values  $E_\mu$ , a different set for each time step. These spectral values are then used in the individual time steps of Bažant's exponential algorithm based on Kelvin chain (as described in Bažant 1971, 1975, 1982, RILEM 1988, Jirásek and Bažant 2002).

For example, the ACI compliance function (ACI 1971), which reads  $J(t, t') = \psi(t')f(\xi)$ , where  $\xi = t - t'$  and  $f(\xi) = \xi^{0.6}/(10 + \xi^{0.6})$ , can be approximated by a continuous retardation spectrum (Bažant and Xi 1995) for a fixed value of the given aging function  $\psi(t')$ ;

$$A_\mu = \psi(t') L(\tau_\mu) \Delta(\log \tau_\mu) \ln 10, \quad L(\tau_\mu) = - \lim_{k \rightarrow \infty} \frac{(-k\tau_\mu)^k}{(k-1)!} f^{(k)}(k\tau_\mu) \quad (2)$$

where  $k$  is a positive integer, and  $f^{(k)}$  represents  $k$ -th order derivative of function  $f(\xi)$  ( $k = 3$  usually suffices for good accuracy).

In Fig. 3 (top), two sets of constant moduli of Kelvin chain obtained by approximating the continuous spectrum are used to approximate the compliance function  $J(t, t')$  corresponding to sustained stress applied at age  $t' = 7$  days (diamond points) or 210 days (circle points). As seen, the difference from the  $J(t, t')$  curves is negligible, compared to the ACI model. In advance of the step-by-step finite element analysis, the spectrum and the corresponding set of Kelvin chain moduli  $E_\mu$  is identified from the given compliance function for the center of each time step.

The corresponding spectra  $A_\mu$  ( $\mu = 1, 2, 3, \dots$ ) are also plotted in Fig. 3 (middle). Note that in each case the spectrum  $A_\mu$  approaches 0 as the retardation time  $\tau_\mu$  increases. The reason is that the creep strain expressed by ACI model is bounded, with the creep rate essentially vanishing

after 10 years (this is, of course, contradicted by long-term creep test results, e.g., Brooks 1984, 2005). The surface of the continuous spectra  $A_\mu = 1/E_\mu$  that closely approximates the ACI compliance function for different ages at loading is exemplified in Fig. 3 (bottom) (where the coordinates are the retardation times  $\tau_\mu$ , and the ages  $t'$ ). For the CEB, JSCE and GL, the procedure is similar.

For model B3, which is based on solidification theory, the moduli of Kelvin chain are constant, but only for basic creep. As demonstrated in Fig. 4 (top), the creep compliances for ages  $t' = 7$  days (diamonds) and 210 days (circles) can be closely approximated by same non-aging spectrum, which is plotted in the middle of Fig. 4. Besides the basic creep, there is in model B3 a separate drying creep term, which captures the Pickett effect. This term applies only to the in-plane directions, and so different compliance functions had to be obtained for the in-plane and transverse directions of the plates. The drying creep term of model B3 applies only to the normal strains and causes no Poisson effect. These distinctions cannot be made for the other models. Unlike the basic creep, which is unbounded, the drying creep is bounded. Like the shrinkage, it depends on humidity and cross section thickness.

The microprestress-solidification theory (Bažant et al. 1997), would have been more realistic for representing both the drying creep and aging. However, it would have required calculating the distributions of pore relative humidity across the thickness of each slab, which would have necessitated not one but at least six finite elements over the slab thickness.

In model B3, the drying creep is approximated by the compliance function

$$C_d(t, t', t_c) = q_5 \sqrt{e^{-8H(t)} - e^{-8H(t')}} \quad H(x) = 1 - (1 - h) \tanh \sqrt{\frac{x - t_c}{\tau_{sh}}} \quad (3)$$

where  $t$  = current age of concrete,  $t'$  = age at loading,  $t_c$  = curing time,  $h$  = relative humidity, and  $\tau_{sh}$  = shrinkage halftime. As seen from Eq. (3), a non-aging spectrum cannot be identified to approximate the drying creep. Therefore, age-dependent spectrum similar to Eq. (3) is calculated. The spectrum  $A_\mu$ , describing the drying creep, is plotted in Fig. 4 (bottom). It can be seen that the age-dependent spectrum approaches zero as the retardation time  $\tau_\mu$  increases. This is because the drying creep is bounded. Contrary to the non-aging spectrum for basic creep, it reaches a finite value as  $\tau_\mu$  increases. Therefore, the overall long-time creep predicted by model B3 will follow a constant slope when plotted in the logarithmic scale.

As it transpired from recent research (Bažant 2000) and current study, the models other than B3 exhibit some serious deficiencies, theoretical as well as practical. One deficiency, especially for the ACI and CEB models, is that the long-time creep is strongly underestimated. Another deficiency of the ACI model, and to a lesser extent the CEB model, is that the drying creep, which is very sensitive to the cross section thickness, is not separated from the basic creep, and that the effects of thickness on shrinkage and on drying creep are described by a scaling factor rather than by a time delay (Bažant 2000).

After the Kelvin chain moduli for the current time step  $\Delta t$  and current integration point are obtained, the exponential algorithm (Bažant 1975, 1982; RILEM 1988; Jirásek and Bažant 2002) is implemented. It was derived as the exact solution for stress varying linearly within  $\Delta t$  (Bažant 1971). While the standard central or backward difference algorithm becomes numerically unstable for  $\Delta t$  exceeding the shortest  $\tau_\mu$ , this algorithm is unconditionally stable. The initial time steps  $\Delta t$  after the hinge installation at midspan were 0.1, 1, 10 and 100 days. After that,  $\Delta t$  was kept constant at 100 days up to 19 years. For the deflection prediction up to 150 years, all the subsequent  $\Delta t$  were 1000 days. Although time steps increasing in geometric progression would have been computationally more efficient, they would not have matched the times of deflection measurements.

## Comparison to Bending Theory with Plane Cross Sections

The existing computer programs for creep effects assume the prestressed concrete box girders to follow the engineering theory of bending, which presume the cross sections of the box to remain planar and normal to the deflection curve. However this theory is too simplified to capture the three-dimensional deformation of box girders. The main deficiency is that it misses significant shear lag effect in the top slab, in the webs and in the bottom plate, each of which is different for the self weight and for the prestress loads from tendon anchors. See in Fig. 5 the distribution of normal and shear stress in the cross section located at 14.63 m (48 ft.) from the main pier under self weight, and in the cross section at 60.35 m (198 ft.) from the main pier under prestress.

A strong sensitivity to errors is caused by the fact that the bridge deflection represents a small difference between two large numbers—the downward deflection due to the self weight and the upward deflection due to the prestress. The shear lag plays a relatively more important role in the former. The error due to neglecting the shear lags is thus magnified.

Fig. 6 shows that the discrepancy between the full three-dimensional analysis and the analysis based on the engineering theory of bending is significant. The deflections and prestress losses for both cases are compared using the B3 and ACI models. Compared to the three-dimensional analysis, the analysis using the classical bending theory is found to underpredict the deflection by about 20%.

In the KB Bridge design, an approximate correction for the shear lag in the top slab due to self weight was introduced (Shawwaf 2008) through the classical effective width concept (Reissner 1946, Benscoter 1954, Abdel-Samad et al. 1968, Malcolm and Redwood 1970, Richtlinien 1973). However, these classical formulas are not very accurate and still miss the shear lags in the webs and bottom slabs and those due to prestress forces. This causes a significant error.

## Cyclic Creep and Its Structural Effect

In the discussions at various conferences it has often been claimed that the cyclic creep caused by repeated traffic loads may explain the excessive long time deflection. Let us examine these claims.

As argued in Bažant and Kim (1992), the cyclic creep caused by repeated traffic loads may best be represented as an acceleration of the basic creep due to sustained load. The acceleration of creep by a compressive stress cycled between limits  $\sigma_{min}$  and  $\sigma_{max}$  may be represented as a forward shift,  $\Delta t_N$ , of the time for which the deformations are evaluated. According to empirical Eq. 3 in Bažant and Kim (1992) (also see Bažant and Panula 1979),

$$\Delta t_N = 2\pi N \tau_c F^3(s) (\sigma_{max}/f'_0)^2 \Delta^2 \quad (4)$$

where  $f'_0$  = compressive strength at the time of loading (estimated as 25.2 MPa, or 3658 psi for the KB Bridge);  $\Delta = (\sigma_{max} - \sigma_{min})/f'_0$ ;  $\tau_c \approx 15$  days;  $F(s) = (1 + 3s^5)/(1 - s^{10})$ ;  $s = \bar{\sigma}/f'_0$ ; and  $\bar{\sigma}$  = time average stress due to all loads.

At the centroid of the bottom slab at the face of the pier,  $\sigma_{min} = 7.50$  MPa (1088 psi). The most important traffic loads are heavy trucks, considered to weigh about 20 tons (44092 lb). The stress caused by each of them is calculated to be about 0.21 MPa (30.5 psi), and so  $\sigma_{max} = 7.71$  MPa (1118.5),  $F(s) = 1.00$ . It is estimated that only about 1 million such trucks passed the bridge within 18 years, i.e.  $N = 10^6$ . For the KB Bridge, the intervals between such heavy trucks were so long that the time average of the cyclic stress component was negligible and  $\bar{\sigma} \approx \sigma_{min}$  = stress caused by all permanent loads (self-weight, prestress and additional dead load). Substitution of these numbers into Eq. (4) yields:

$$\Delta t_N = 2\pi 10^6 \times (15 \text{ days}) \times 1^3 \times (7.71/25.2)^2 (0.21/25.2)^2 = 612 \text{ days} \quad (5)$$

So the effect of cyclic creep due to the heavy trucks is equivalent to extending the duration of static creep by about 612 days. In this calculation, it was assumed that only one 20 ton truck would appear at the mid-span at the same time. The number of simultaneous occurrences of 2 or 3 such trucks at the mid-span is estimated to be  $N = 10000$  or 1000, respectively (during 18 years), and similar calculations then show that the cyclic creep produced is equivalent to extending the static creep duration by 26 days or 6 days, respectively.

Traffic observations further showed that about 200 regular cars, of about 3 tons each, passed the bridge per hour during daytime. This gives  $N = 16$  million car passages in 18 years. Similar calculations give the extension of 210 days.

All these extensions together amount to about 854 days of static creep for the cross section at the face of the pier. From this, one can determine the additional cyclic creep strain in the bottom plate.

Similar calculations can be repeated for the forward time shifts of cyclic creep strain history at various points of the web and top plate of the cross section at the face of pier. Since both  $\sigma_{max}$  and  $\Delta$  are smaller, the forward shift of the creep history at these points will be smaller than 854 days. Hence, 854 days is the upper bound for the forward shift of the curvature history of the girder at this cross section. Calculations for the quarter-span cross section gives a slightly longer time shift, but the effect of curvature increase on the midspan deflection is for the quarter-span cross section much smaller than it is for the cross section at the pier face. Consequently, the upper bound on the forward time shift of the midspan deflection history should be roughly the same as the upper bound on the shift of the curvature history in the cross section at the pier face. Looking at the terminal slope of the deflection curve of the bridge in Fig. 4 of Part I, which is about 1 m per 15000 days, one concludes that the cyclic creep increased the midspan deflection by not more than  $1 \text{ m} \times 854/15000 = 5.7 \text{ cm}$ . Compared to the total observed deflection of 1.61 m, this is not important.

For bridges of shorter spans, in which the self weight represents a smaller portion of the load, the cyclic creep effect can be more important. But it can hardly be major. For example, the Nusle Valley Bridge in Prague (Bažant 1968a, 1968b), which has spans 102 m and carries a heavier traffic load (subway trains inside the box in addition to cars on top) was analyzed (by a different method) in 1966. It was concluded that the cyclic creep would increase the deflection of that bridge by only 4 cm (Bažant 1968b).

The present model of cyclic creep analysis was formulated in Bažant and Panula (1979) and refined in Bažant and Kim (1992), where the model was also validated by comparisons with the main existing data (Gaede 1962, Kern and Mehmel 1962, Whaley and Neville 1973, Sutter and Mickleborough 1975, Hirst and Neville 1977). Note that the present cyclic creep correction cannot be applied to the ACI, CEB and JSCE models. They would give a zero effect of cyclic creep because the creep load-deflection curve terminates with a horizontal asymptote.

This analysis also brings about another interesting point. Since (aside from the nonlinear corrections for drying and cracking), the principle of superposition is the basis of creep analysis, the time average of traffic loads should be included in the permanent loads. This effect, neglected so far, might be non-negligible for bridges with many lanes, with both a highway and a railroad, or with a dense traffic of heavy trucks.

## Lessons Learned and Recommendations

1. As a purely predictive tool, none of the available material models for predicting creep and shrinkage is satisfactory.
2. The 1971 ACI model (reapproved in 2008), and to a somewhat lesser extent the CEB and JSCE models, severely underestimate multi-decade deflections as well as the prestress losses, and give an unrealistic shape of deflection histories. The recent GL model gives better predictions, but not sufficiently better. None of these models has free intrinsic

input parameters to be updated from experiments or to explore the range of possible responses, and none can take temperature into account.

3. Model B3, which is to a large extent theoretically based and has been calibrated by filtering out the database bias for short durations and ages, gives significantly better multi-decade predictions of deflection history and its shape, and of deflection growth rate.
4. Even model B3 is unsatisfactory when its input parameters are estimated from the composition of concrete or taken at their default values. However, thanks to its free parameters, model B3 can be made to fit the measurements perfectly with input parameters that are within their realistic range, agreeing with the long-term test data that exist. Thus the form of model B3 appears to be correct, and the problem is with the empirical formulas predicting the input parameters from the composition of concrete. Obviously, these formulas can, and should, be improved.
5. The box girders are thick-walled shells for which the beam-type analysis is inadequate. Three-dimensional analysis must be used. Its main purpose is to capture the shear lag effects, which are rather different for self weight and for the loads from prestressing tendons, and occur not only in the top slab but also in the webs and the bottom slab. At the piers, the self weight produces large vertical shear forces in the web, while the prestress does not, while the loads from tendon anchors produce shear lags mainly in the top slab. The shear lag for the self weight is stronger than it is for the prestress. Since the total deflection is a small difference of two large numbers, one for the downward deflection due to self-weight and the other for the upward deflection due to prestress, small percentage errors in each (typically  $\pm 10\%$  to  $15\%$ ) will result in a far larger percentage error in the total deflection.
6. For box girders wider than the KB Bridge (which had only two lanes), the difference between the beam type analysis of creep and shrinkage and the three-dimensional analysis which captures the shear lag effects must be expected to be larger.
7. The effect of thickness differences among the webs and the top and bottom slabs on the drying shrinkage and drying creep must be taken into account. This leads to non-uniform creep and shrinkage properties throughout the cross section, manifested as differential drying creep compliances and differential shrinkage.
8. In the creep and shrinkage prediction model, the drying creep should be separated from the basic creep, because the former is thickness dependent and approaches a finite terminal value while the latter is thickness independent and unbounded. Only model B3 has this feature. As evidenced by the KB Bridge, the thickness-induced differences in the compliance functions for drying creep can be more important than those in shrinkage.
9. The prestress loss in box girders can be 2 to 3 times higher than predicted by simple textbook formulas or lump estimates. It can also be much higher than that calculated by the theory of beam bending in which the cross sections are assumed to remain plane. It should be calculated as part of the three-dimensional finite element analysis of stresses and deflections.
10. When dealing with large creep-sensitive structures, the creep and shrinkage prediction model must be updated by means of short-time tests of the creep and shrinkage of the given concrete. The updating is effective only if the curves of creep and shrinkage growth have correct shapes for short times, which is the case only for model B3.
11. The shrinkage tests must be accompanied by simultaneous measurements of water loss due to drying (Bažant and Baweja 1995,2000), or else the extrapolations can have errors of the order of 100% (the value of such tests has been demonstrated for some recent large bridges; Navrátil 1998). B3 is a model that has been specifically formulated so as to allow easy updating by linear regression, while for other models the updating problem is nonlinear.

12. Large bridges should be designed not for the mean but for the 95% confidence limit on the predicted deflection (in other words, having to repair or close only 1 among 20 similar bridges is acceptable, but 10 is not). The necessary statistical analysis is easy. It suffices to repeat a deterministic computer run of structural response about 10 times, using random samples of the input parameters. Since the distribution of structural response can be assumed to be normal, it suffices to obtain from the structural responses only the mean and the coefficient of variation.
13. As observed in an earlier study (Křístek et al. 2006), the deflection evolution of large box girders is usually counterintuitive. The deflections at first grow slowly or are even negative, which may lead to unwarranted optimism, but after a few years a rapid and excessive deflection growth sets in. The early deflections of the KB bridge were not measured, but according to the present computer simulations with non-symmetric drying, the deflection growth of this bridge must have been very slow during the first year (Fig. 3, Part I).
14. In design it is prudent to minimize deflections and prestress losses by the following measures, most of which are well known though often not followed: 1) avoid mid-span hinge; 2) choose a concrete with a low long-time creep; 3) use a tendon layout that minimizes deflections (Křístek et al. 2008); 4) give concrete more time to gain strength before prestressing; 5) increase the level of prestress, preferably so high that an upward deflection be predicted (Fig. 7); 6) use stiffer (deeper) girders (Fig. 7); and 7) install empty ducts for possible later installation of additional tendons.

**Acknowledgment:** Financial support from the U.S. Department of Transportation through Grant 0740-357-A222 from the Infrastructure Technology Institute of Northwestern University, is gratefully appreciated. Thanks are due to Khaled Shawwaf of DSI, Inc., Bolingbrook, Illinois, for providing valuable information on the analysis, design and investigations of this bridge, to Man-Chung Tang and Mirek Olmer of T.Y. Lin International, and Brian McDonald of Exponent Failure Analysis Associates, Menlo Park, for some further valuable comments, and to Yasumitsu Watanabe of Shimizu Co., Tokyo, and Lukáš Vráblík of CTU Prague for graciously providing the data on four Japanese bridges and on Děčín Bridge.

## Appendix: Algorithm and Numerical Implementation

### Basic Notations

$h$  = environmental humidity,  $T$  = temperature;  $\mathbf{D}$  = constant  $6 \times 6$  elastic stiffness matrix for isotropic material with a given Poisson ratio  $\nu$  and a unit value of Young's modulus.

$E_0$  = conventional short-time elastic modulus of concrete for all models except model B3 for which  $E_0 = 1/q_1$  = asymptotic modulus (i.e., modulus extrapolated to load duration  $10^{-9}$  s);

$E''$  = incremental modulus of quasi-elastic stress-strain relation;

$t_{n+1/2} = t_0 + [(t_n - t_0)(t_{n+1} - t_0)]^{1/2}$  = mid-points of time intervals in log-scale;

$t_n$  ( $n = 1, 2, \dots$ ) = chosen discrete times;

$\Delta t = t_{n+1} - t_n$  = time steps;

$\boldsymbol{\epsilon}, \boldsymbol{\sigma}$  = vectors ( $6 \times 1$  column matrices) of strain and stress;

$\boldsymbol{\epsilon}_s$  = vector ( $6 \times 1$  column matrix) of shrinkage strain;

$\Delta \boldsymbol{\epsilon}''$  = vector ( $6 \times 1$  column matrix) of inelastic strain increments;

$\tau_\mu = 10^{-7+\mu}$  = discrete retardation times,  $\mu = 1, 2, \dots, N$ ;

$\sigma_i$  = principal stresses ( $i = 1, 2, 3$ )

### Algorithm Utilizing ABAQUS (Applicable to Every Creep Model)

1. For each integration point of each finite element, specify effective slab thickness  $t_b$ , relative humidity  $h$  and temperature  $T$  (but, if  $h$  and  $T$  are variable, update them at the start of each time step).
2. For curing time  $t = t_c$ , initialize the vector ( $6 \times 1$  column matrix) of shrinkage strains  $\epsilon_s^0$ .
3. For  $t = t_0$ , initialize the internal variables  $\gamma_\mu^{(0)} = 0$  ( $\mu = 1, \dots, N$ ) and set  $J(t_0, t_0) = 1/E_{t_0}$  (where  $E_{t_0}$  = conventional short-time elastic modulus at age of loading). However, in the special case of model B3, set  $J(t_0, t_0) = q_1$  (= asymptotic modulus).
4. Select the discrete retardation times  $\tau_\mu = 10^{\mu-7}$  days,  $\mu = 1, 2, \dots, N$  where, for lifespan  $< 250$  years,  $N = 13$  satisfies the condition that  $10^{N-7}$  days  $\approx 10 \times$  lifespan (see Note I).
5. Loop over time steps (separated by discrete times  $t_n$ ,  $n = 1, 2, \dots$ ). Set  $\Delta t = t_n - t_{n-1}$ , and  $t_{n-1/2} = t_0 + [(t_n - t_0)(t_{n-1} - t_0)]^{1/2}$  for  $n > 1$ . For  $n = 1$ ,  $t_{1/2} = (t_0 + t_1)/2$ .
6. Loop over finite elements and their integration points.
7. In user subroutine *uexpan*, calculate from  $t_b, h$  and  $T$ , for each integration point, the increment of the shrinkage strain vector ( $6 \times 1$  column matrix)  $\Delta \epsilon_s = \epsilon_s(t_n) - \epsilon_s(t_{n-1})$
8. Supply current stress  $\sigma^{(n-1)}$  and strain increment  $\Delta \epsilon = \Delta \epsilon^{total} - \Delta \epsilon_s$ , as calculated by ABAQUS, to the user material subroutine in *umat*, in which Bažant's exponential algorithm is implemented.
9. Calculate the continuous retardation spectrum by applying Widder's formula (which represents Laplace transform inversion):  

$$L(\tau_\mu) = -\lim_{k \rightarrow \infty} (-k\tau_\mu)^k C^{(k)}(k\tau_\mu) [(k-1)!]^{-1}.$$
 Here  $C^{(k)}$  =  $k$ -th order derivative on  $t$  of the creep part  $C(t, t_{n-1/2})$  of the compliance function,  $C(t, t') = J(t, t') - 1/E_0$  (usually  $k = 3$  suffices for good enough approximation).
10. Determine the discretized spectrum, different in each integration point of each finite element:  

$$A(\tau_\mu) = L(\tau_\mu) \ln 10 \Delta(\log \tau_\mu) = L(\tau_\mu) \ln 10.$$
11. Calculate, for each integration point of each finite element, parameters:  

$$\beta_\mu = e^{-\Delta t / \tau_\mu}, \lambda_\mu = \tau_\mu(1 - \beta_\mu) / \Delta t, D_\mu = [A(\tau_\mu)(1 - \lambda_\mu)]^{-1};$$
 and the incremental modulus:  

$$E''(t_{n-1/2}) = [E_0^{-1} + \sum_{\mu=1}^N D_\mu^{-1}]^{-1}.$$
12. Calculate, for each integration point of each finite element, the inelastic (creep) strain increment vector:  

$$\Delta \epsilon'' = \sum_{\mu=1}^N (1 - \beta_\mu) \gamma_\mu^{(n-1)}.$$
13. Check the tensile strength limit:  $\sigma_i \leq f'_t$  (where  $\sigma_i$  = principal stresses,  $i = 1, 2, 3$ ). If exceeded for any  $i$ , adjust either  $E''$  or  $\Delta \epsilon''$  accordingly (although usually unnecessary, the compressive damage could also be included here).
14. Supply to ABAQUS finite element program for this integration point at this time step the  $6 \times 6$  and  $6 \times 1$  matrices figuring in the incremental quasi-elastic matrix stress-strain relation  

$$\Delta \sigma = E'' \mathbf{D} (\Delta \epsilon - \Delta \epsilon'')$$
 where  $\mathbf{D}$  is a constant  $6 \times 6$  matrix for isotropic material with given Poisson ratio  $\nu$ .
15. End of loops over finite elements and over their integration points (return to step 6 unless computations have been run for the last integration point).
16. Assemble the incremental stiffness matrix and load matrix of the structure.
17. Run with ABAQUS the incremental elastic finite element analysis, in which each integration point has generally a different (non-isotropic) elastic moduli matrix and a different (non-isotropic) inelastic strain vector, as calculated above.

18. Start a new loop over finite elements and their integration points.
19. After retrieving ABAQUS results for the stress and displacement increments, update the total deflections and also the internal variable vectors:  

$$\boldsymbol{\gamma}_\mu^{(n)} = \lambda_\mu \Delta \boldsymbol{\sigma} \mathbf{D}_\mu^{-1} + \beta_\mu \boldsymbol{\gamma}_\mu^{(n-1)}.$$
20. End of loop over finite elements and their integration points. Return to 18, but if the last integration point has been handled, return to 5 and begin the next time step  $\Delta t$  unless the specified lifespan has been reached.

*Note I:* The number,  $N$ , of internal variables could actually be reduced to about 5. But then the first  $L(\tau_\mu)$  would have to be computed as the integrated area under the spectrum up to  $-\infty$  in the log-time scale (the reason is that Kelvin units with  $\tau_\mu \ll \Delta t$  behave as springs, and the compliances of springs coupled in series can be combined into one compliance). Using  $N = 22$  for model B3 and  $N = 13$  for other models increases the demand on computer time and storage but is simpler to program. The spectral values  $L(\tau_\mu)$  for  $\tau_\mu \gg t$  (the current time) can be ignored since the corresponding Kelvin units behave as perfectly rigid.

### Exponential Algorithm Simplifications for Model B3

The foregoing algorithm can also be used for model B3, provided that  $J(t, t')$  is computed for each integration point. However, for basic creep there exists a simpler exponential algorithm (Bažant and Prasannan 1989a,b) which needs only the compliance rate  $\dot{J}(t, t')$  and is applied only to the non-aging viscoelasticity of the nonaging constituent of growing volume. The following steps are then modified:

1. In Steps 1–4,  
 $\mu^b = 1, 2, \dots, N^b$ ,  $\tau_\mu^b = 10^{-15+\mu^b}$  and  $\mu^d = 1, 2, \dots, N^d$ ,  $\tau_\mu^d = 10^{-7+\mu^d}$ .  
Here  $N^b = 22$  and  $N^d = 15$  ( $\tau^b$ ,  $\tau^d$  = retardation times for basic creep and drying creep).
2. In Step 10, for basic creep, replace  $A(\tau_\mu)$  with  

$$A^b(\tau_\mu^b) = (\sqrt{1/t_{n-1/2} + q_3/q_2}) A(\tau_\mu^b);$$
where  $A^b(\tau_\mu^b)$  is the discretized spectrum for basic creep, and time  $t_{n-1/2}$  must be in days (see Eq. 13 in Bažant and Prasannan 1989a).
3. In Steps 11–12,  

$$\Delta \boldsymbol{\epsilon}'' = \sum_{\mu=1}^{N^b} (\sqrt{1/t_{n-1/2} + q_3/q_2}) \times (1 - \beta_\mu) \boldsymbol{\gamma}_\mu^{(n-1)} + \sum_{\mu=1}^{N^d} (1 - \beta_\mu) \boldsymbol{\gamma}_\mu^{(n-1)}.$$
4. After Step 12, add the strain increment due to the viscous flow:  

$$\Delta \boldsymbol{\epsilon}'' \leftarrow \Delta \boldsymbol{\epsilon}'' + q_4 \boldsymbol{\sigma}^{(n-1)} \Delta t / t_{n-1/2}.$$

### Implementation Example Using ACI-209 Model

For ACI model,

$$J(t, t') = (1 + \phi(t, t')) / E(t'), \quad \phi(t, t') = 2.35 \gamma_c (t - t')^{0.6} / [10 + (t - t')^{0.6}]$$

where  $\gamma_c$  = empirical factor accounting for age  $t'$  at loading, humidity, slab thickness, slump of fresh concrete, and contents of fine aggregates and of air. In ABAQUS, the exponential algorithm is used in the user material subroutine, as follows:

1. At  $t = t_0$ , initialize the internal variables:  
 $\boldsymbol{\gamma}_\mu^{(0)} = 0$ ,  $J(t_0, t_0) = 1/E(t_0)$   
where  $t_0$  = time when the first load is applied. Select  $\tau_\mu = 10^{-7+\mu}$  ( $\mu = 1, 2, \dots, 13$ ).
2. Use Widder's formula to calculate the continuous spectrum:  

$$d^3 \phi / d\xi^3 = \psi(\xi) = 2.35 \gamma_c [0.336 \xi^{-2.4} (10 + \xi^{0.6})^{-1} + 0.528 \xi^{-1.8} (10 + \xi^{0.6})^{-2} + 0.432 \xi^{-1.2} (10 + \xi^{0.6})^{-3} - 1.296 \xi^{-0.6} (10 + \xi^{0.6})^{-4}]$$
where

$\xi = t - t'$ ;  $L(\tau_\mu) = 2.35\gamma_c(3\tau_\mu)^3\psi(3\tau_\mu)/2$   
 where  $\gamma_c$  is calculated using  $t_{n-1/2}$ .

3. Discretized spectrum:

$$A(\tau_\mu) = L(\tau_\mu) \ln 10 / E(t_{n-1/2}).$$

4. Calculate:

$$\beta_\mu = e^{-\Delta t / \tau_\mu}, \lambda_\mu = \tau_\mu(1 - \beta_\mu) / \Delta t,$$

$$D_\mu = [A(\tau_\mu)(1 - \lambda_\mu)]^{-1}.$$

The effective modulus then is:

$$E''^{-1}(t_{n-1/2}) = E^{-1}(t_{n-1/2}) + \sum_{\mu=1}^N D_\mu^{-1}.$$

5. Creep strain increment:

$$\Delta \epsilon'' = \sum_{\mu=1}^N (1 - \beta_\mu) \gamma_\mu^{(n-1)}.$$

6. The stress-strain relation for this integration point is:

$$\Delta \sigma = E''(t_{n-1/2}) \mathbf{D}(\Delta \epsilon - \Delta \epsilon'').$$

The loop repeats these calculations for all the integration points of all finite elements and supplies the stiffness and load matrices of the incremental stress-strain relations for the assembly of the structural stiffness and load matrices. Then ABAQUS can run the incremental elastic finite element analysis.

7. After retrieving the stress increments computed by ABAQUS, update for each finite element the internal variables:

$$\gamma_\mu^{(n)} = \lambda_\mu \Delta \sigma \mathbf{D}_\mu^{-1} + \beta_\mu \gamma_\mu^{(n-1)},$$

Then begin the next time step unless the lifetime has been reached.

To check programming of the creep law with the exponential algorithm, the following results should be obtained: For  $\gamma_c = 1.25(t')^{-0.118}$ ,  $E_e = E_{28}\sqrt{t}/(4 + 0.85t)$  where  $E_{28} = 30$  GPa, and uniaxial loading by  $\sigma = 1$  MPa applied at  $t_0 = 7$  days, the results are  $\epsilon = 4.92 \times 10^{-5}$  for  $t = 8$  days;  $\epsilon = 9.68 \times 10^{-5}$  for  $t = 100$  days;  $\epsilon = 0.00012$  for  $t = 1000$  days and  $\epsilon = 0.000129$  for  $t = 10000$  days. These are almost the same results as obtained directly from the ACI formula.

## References

- [1] ABAM Engineers Inc. (1993). *Basis for design, Koror-Babeldaob bridge repairs*, submitted to Bureau of Public Works, Koror, Republic of Palau, October, 1993.
- [2] Abdel-Samad, S.R., Wright, R.N., and Robinson, A-R. (1968). "Analysis of Box Girders with Diaphragms". *J.Struct. Div., Proc. ASCE* 94(ST10), pp. 2231-2255.
- [3] ACI Committee 209 (1971) "Prediction of creep, shrinkage and temperature effects in concrete structures" *ACI-SP27, Designing for Effects of Creep, Shrinkage and Temperature*, Detroit, pp. 51-93.
- [4] ACI Committee 209 (2008). *Guide for Modeling and Calculating Shrinkage and Creep in Hardened Concrete* ACI Report 209.2R-08, Farmington Hills.
- [5] Bažant, Z.P. (1967) "Linear creep problems solved by a succession of generalized thermoelasticity problems" *Acta Technica ČSAV*, 12, pp. 581-594.
- [6] Bažant, Z.P. (1968a). "Langzeitige Durchbiegungen von Spannbetonbrücken infolge des Schwingkriechens unter Verkehrslasten" (Long-time deflections of prestressed concrete bridges due to cyclic creep under traffic loads), *Beton und Stahlbetonbau*, 63, 282-285.
- [7] Bažant, Z.P. (1968b). "On causes of excessive long-time deflections of prestressed concrete bridges. Creep under repeated live load" (in Czech), *Inženýrské Stavby*, 16, 317-320.
- [8] Bažant, Z.P. (1971). "Numerically stable algorithm with increasing time steps for integral-type aging creep." Proc., *First Intern. Conf. on Struct. Mech. in Reactor Tech. (SMiRT-1)* (org. by BAM, Berlin, and Commission of Eur. Communities), ed. by T.A. Jaeger, West Berlin, Vol. 4, Part H, 119-126.

- [9] Bažant, Z.P. (1975). “Theory of creep and shrinkage in concrete structures: A précis of recent developments” *Mechanics Today*, ed. by S. Nemat-Nasser (Am. Acad. Mech.), Pergamon Press 1975, Vol. 2, pp. 1–93.
- [10] Bažant, Z.P. (1982). “Mathematical models of nonlinear behavior and fracture of concrete” in *Nonlinear Numerical Analysis of Reinforced Concrete*, ed. by L. E. Schwer, Am. Soc. of Mech. Engrs., New York, 1–25.
- [11] Bažant, Z.P. (2000) “Criteria for rational prediction of creep and shrinkage of concrete” *Adam Neville Symposium: Creep and Shrinkage—Structural Design Effects*, ACI SP–194, A. Al-Manaseer, ed., Am. Concrete Institute, Farmington Hills, Michigan, 237-260.
- [12] Bažant, Z.P. and Baweja, S. (1995). “Creep and shrinkage prediction model for analysis and design of concrete structures: ModelB3” *Materials and Structures* 28, pp. 357–367.
- [13] Bažant, Z.P. and Baweja, S. (2000). “Creep and shrinkage prediction model for analysis and design of concrete structures: Model B3.” *Adam Neville Symposium: Creep and Shrinkage—Structural Design Effects*, ACI SP–194, A. Al-Manaseer, ed., pp. 1–83 (update of RILEM Recommendation published in *Materials and Structures* Vol. 28, 1995, pp. 357–365, 415–430, and 488–495).
- [14] Bažant, Z.P., Hauggaard, A.B., Baweja, S. and Ulm, F.-J. (1997). “Microprestress-solidification theory for concrete creep. I. Aging and drying effects” *Journal of Engineering Mechanics, ASCE*, 123(11), pp. 1188–1194.
- [15] Bažant, Z.P. and Kaplan, M.F. (1996). *Concrete at High Temperatures: Material Properties and Mathematical Models*, Longman (Addison-Wesley), London (2nd printing Pearson Education, Edinburgh, 2002).
- [16] Bažant, Z.P., and Kim, Joong-Koo (1992). “Improved prediction model for time-dependent deformations of concrete: Part 5—Cyclic load and cyclic humidity.” *Materials and Structures (RILEM, Paris)* 25 (147), 163–169.
- [17] Bažant, Z.P., and Li, Yuan-Neng (1997). “Cohesive crack with rate-dependent opening and viscoelasticity: I. mathematical model and scaling.” *Int. J. of Fracture* 86 (3), 247–265.
- [18] Bažant, Z.P., and Panula, L. (1979). “Practical prediction of time-dependent deformations of concrete: Part 6—Cyclic creep, nonlinearity and statistical scatter.” *Materials and Structures (RILEM, Paris)* 12, 175–183.
- [19] Bažant, Z.P. and Prasannan, S. (1988). “Solidification theory for aging creep” *Cement and Concrete Research*, 18(6), pp. 923–932.
- [20] Bažant, Z.P. and Prasannan, S. (1989a). “Solidification theory for concrete creep: I. Formulation” *Journal of Engineering Mechanics ASCE*, 115(8), pp. 1691–1703.
- [21] Bažant, Z.P. and Prasannan, S. (1989b). “Solidification theory for concrete creep: II. Verification and application” *Journal of Engineering Mechanics ASCE*, 115(8), pp. 1704–1725.
- [22] Bažant, Z.P., Sener, S. and Kim, J.K. (1987). “Effect of cracking on drying permeability and diffusivity of concrete” *ACI Materials Journal*, 84, pp. 351–357.
- [23] Bažant, Z.P. and Xi, Y. (1995). “Continuous retardation spectrum for solidification theory of concrete creep” *J. of Engrg. Mech. ASCE* 121 (2), pp. 281–288.
- [24] Benscoter, S.U. (1954). “A theory of Torsion Bending for Multi-cell Beams” *J. Appl. Mech. ASME*, 21(1), pp. 25-34.
- [25] Berger/ABAM Engineers Inc. (1995). *Koror-Babeldaob Bridge modifications and repairs*, October 1995.
- [26] Brooks, J.J. (1984). “Accuracy of estimating long-term strains in concrete.” *Magazine of Concrete Research*, 36(128), 131–145.
- [27] Brooks, J.J. (2005). “30-year creep and shrinkage of concrete.” *Magazine of Concrete Research*, 57(9), 545–556.
- [28] *CEB-FIP Model Code 1990. Model Code for Concrete Structures*. Thomas Telford Services Ltd., London, Great Britain; also published by Comité euro-international du béton (CEB), Bulletins d’Information No. 213 and 214, Lausanne, Switzerland.

- [29] DRC Consultants INC. (1996). *Koror-Babelthuap Bridge: Force Distribution in Bar Tendons*, February, 1990.
- [30] Gaede, K. (1962). “Versuche über die Festigkeit und die Verformungen von Beton bei Druckschwellbeanspruchung.” *Deutscher Ausschluß für Stahlbeton*. Heft 144, W. Ernst & Sohn, Berlin.
- [31] Hirst, G.A., and Neville, A.M. (1977). “Activation energy of concrete under short-term static and cyclic stresses.” *Mag. Concr. Res.* 29 (98), 13–18.
- [32] Japan International Cooperation Agency (1990). *Present Condition Survey of the Koror-Babelthuap Bridge*, February, 1990.
- [33] Jirásek, M. and Bažant, Z.P. (2002). *Inelastic analysis of structures*, John Wiley & Sons, London and New York.
- [34] Kern, E., and Mehmel, A. (1962). “Elastische und plastische Stauchungen von Beton infolge Druckschwell- und Standbelastung”. *Deutscher Ausschluß für Stahlbeton*. Heft 153, W. Ernst & Sohn, Berlin.
- [35] Křístek, V., Bažant, Z.P., Zich, M., and Kohoutková (2006). “Box girder deflections: Why is the initial trend deceptive?” *ACI Concrete International* 28 (1), 55–63. ACI SP-194, 237–260.
- [36] Křístek, V., Vráblík, L., Bažant, Z.P., Li, Guang-Hua, and Yu, Qiang (2008). “Misprediction of long-time deflections of prestressed box girders: causes, remedies and tendon layout” *Proc., CONCREEP-8* (8th Int. Conf. on Creep, Shrinkage and Durability of Concrete, Ise-Shima, Japan), T. Tanabe, ed., Nagoya University; pp. 1291–1295.
- [37] Malcolm, D.J., and Redwood, R.G. (1970). “Shear Lag in Stiffened Box Girders”. *J. Struct. Div., Proc. ASCE* 96(ST7), 1403-14019, July, 1970.
- [38] Mamillan, M. and Lellan, M. (1968). “Le fluage de béton” *Annale Inst. Tech. Bat. Trav. Publics (Suppl.)* 21, No. 246, 847–850, and 23 (1970), No. 270, pp. 7–13.
- [39] Navrátil (1998). “Improvement of accuracy of prediction of creep and shrinkage of concrete” (in Czech). *Stavební Obzor*, No. 2, pp. 44–50.
- [40] Nilson, A.H. (1987). *Design of Prestressed Concrete*, 2nd edition, John Wiley & Sons, New York.
- [41] Reissner, E. (1946). Analysis of Shear Lag in Box Beams by the Principle of Minimum Potential Energy” *Quart. App. Math.* 4(3), pp. 268-278.
- [42] Richtlinien (1973) “ für die Bemessung und Ausführung Massiver Brücken”. *German Standards*, Substitute for DIN 1075, Aug., 1973.
- [43] RILEM Committee TC-69 (1988). “State of the art in mathematical modeling of creep and shrinkage of concrete” in *Mathematical Modeling of Creep and Shrinkage of Concrete*, ed. by Z.P. Bažant, J. Wiley, Chichester and New York, 1988, 57–215.
- [44] Shawwaf, Khaled (Dir., Dywidag Systems International USA, Bollingbrook, Illinois; former structural analyst on KB bridge design team), *Private communication*, September 18, 2008, Chicago.
- [45] Sutter, G.T., Mickleborough, N.C. (1975). “Creep of concrete under cyclically loading dynamic loads.” *Cem. Concr. Res.* 5 (6), 565–576.
- [46] Tschoegl, N.W. (1989). *The phenomenological theory of linear viscoelastic behavior: An introduction*. Springer Verlag, Berlin.
- [47] T.Y.Lin International (1996). *Collapse of the Koror-Babelthuap Bridge, Report, T.Y.Lin International*, October, 1996 (32 pp.).
- [48] Whaley, C.P., and Neville A.M. (1973). “Non-elastic deformation of concrete under cyclic compression.” *Mag. Concr. Res.* 25 (84), 145–154.

## List of Figures

1	Three-dimensionally meshed model of KB Bridge and grouped segments. . . . .	17
2	Strain-stress relation if tensile strength is exceeded. . . . .	17

3	Retardation spectra of ACI model. . . . .	17
4	Retardation spectrum of model B3. . . . .	17
5	Shear stress distribution in the cross-section at the main pier, and stress-strain relations for smeared tensile cracking. . . . .	17
6	Comparison of deflections obtained by full three-dimensional analysis with deflections obtained according to the bending theory with cross sections remaining plane. . . .	17
7	Stress profiles for small spans (a) and large spans (b,c), and precautionary design (c). . . .	17

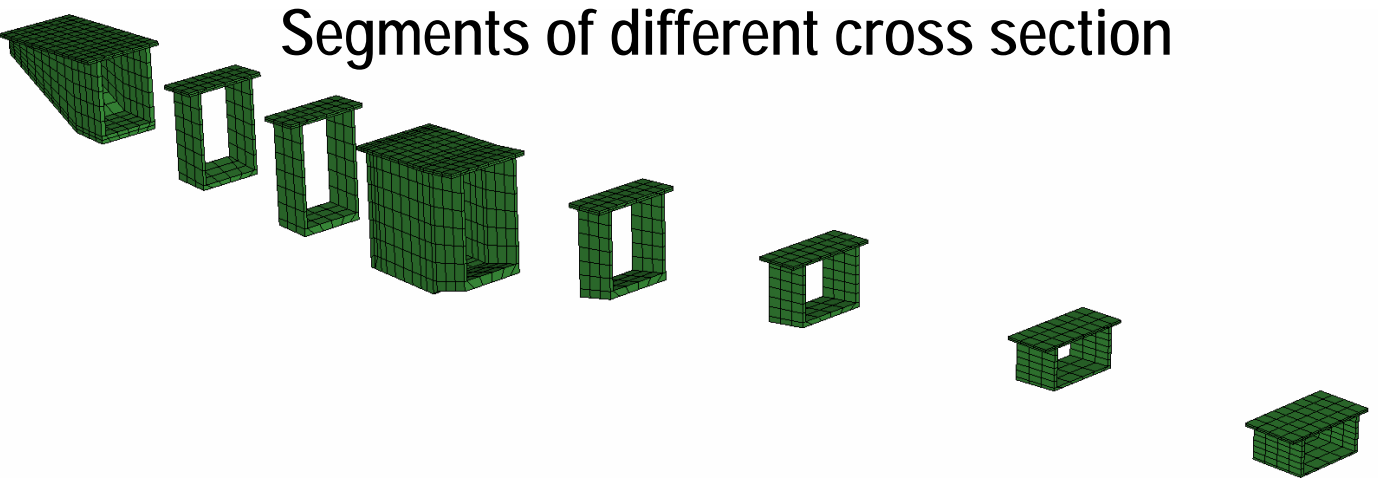
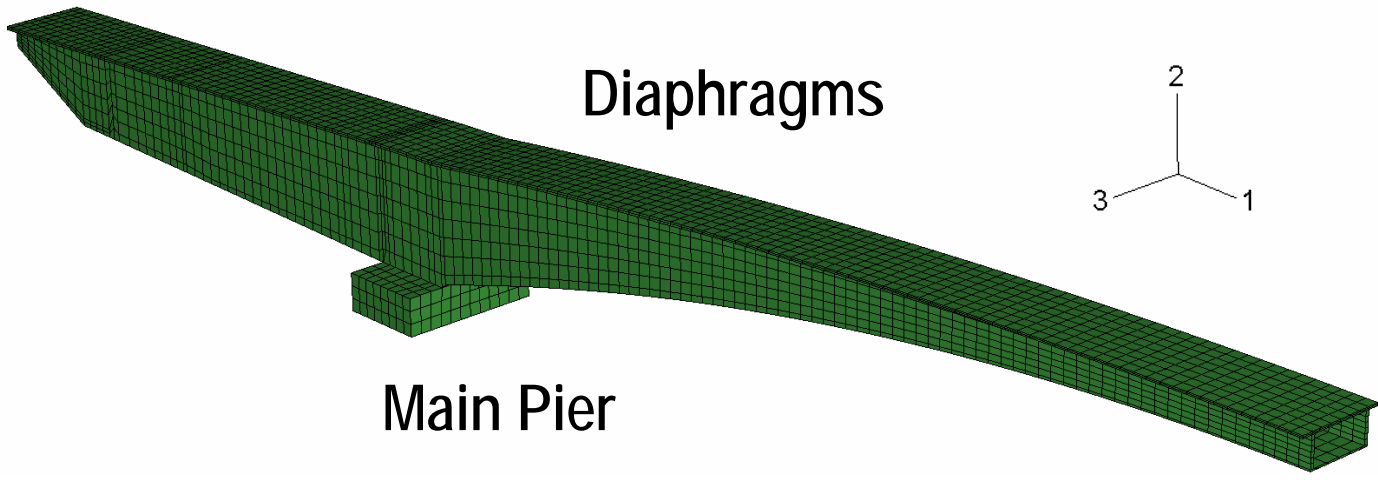


Fig. 1

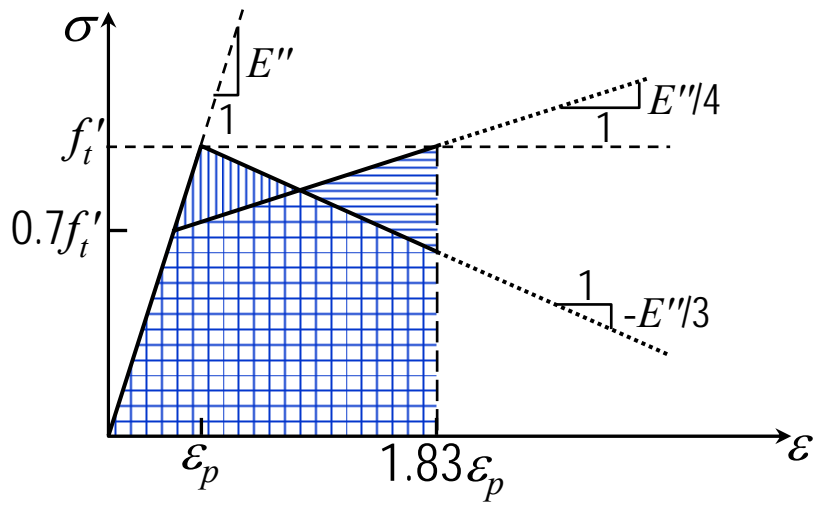


Fig. 2

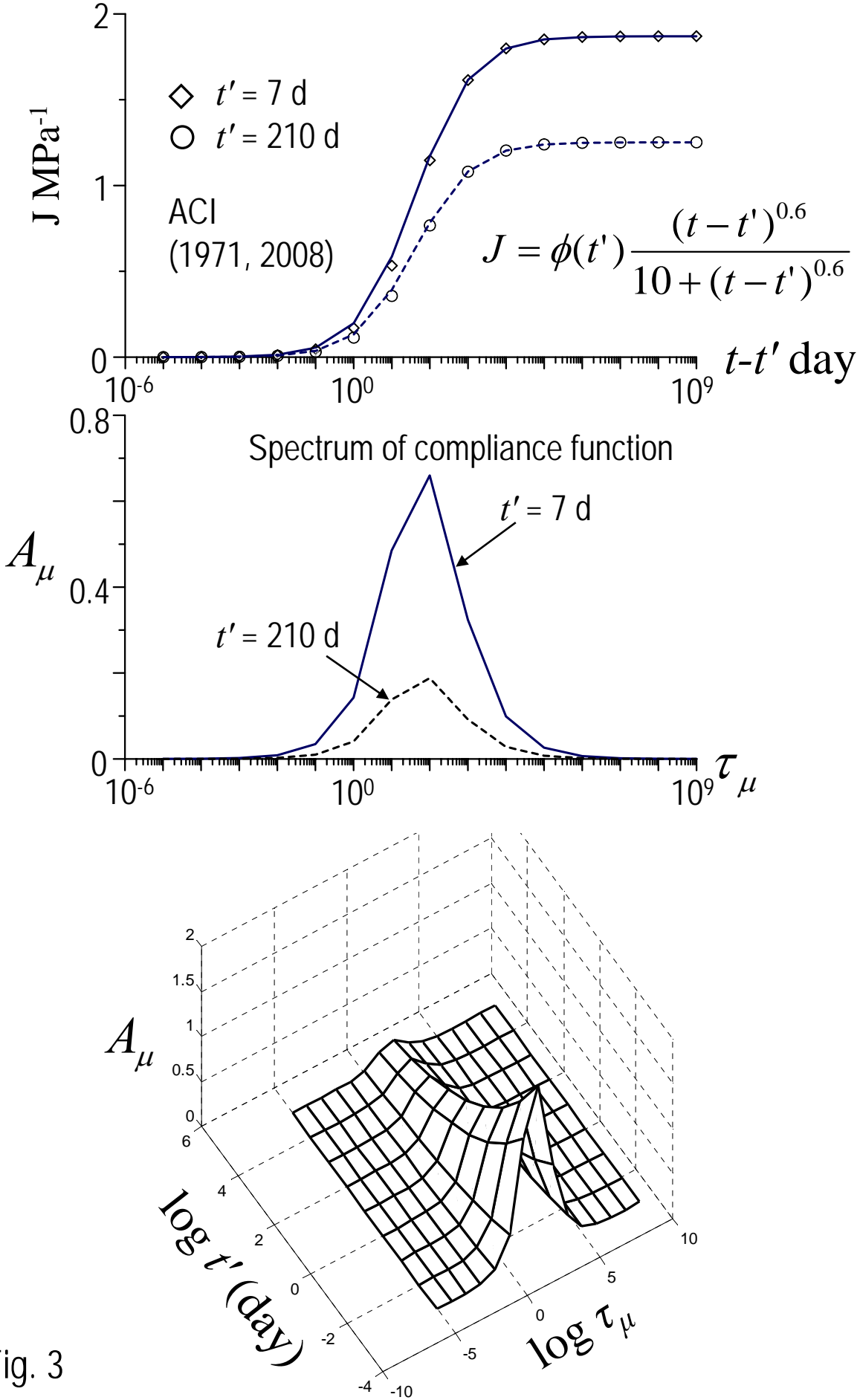
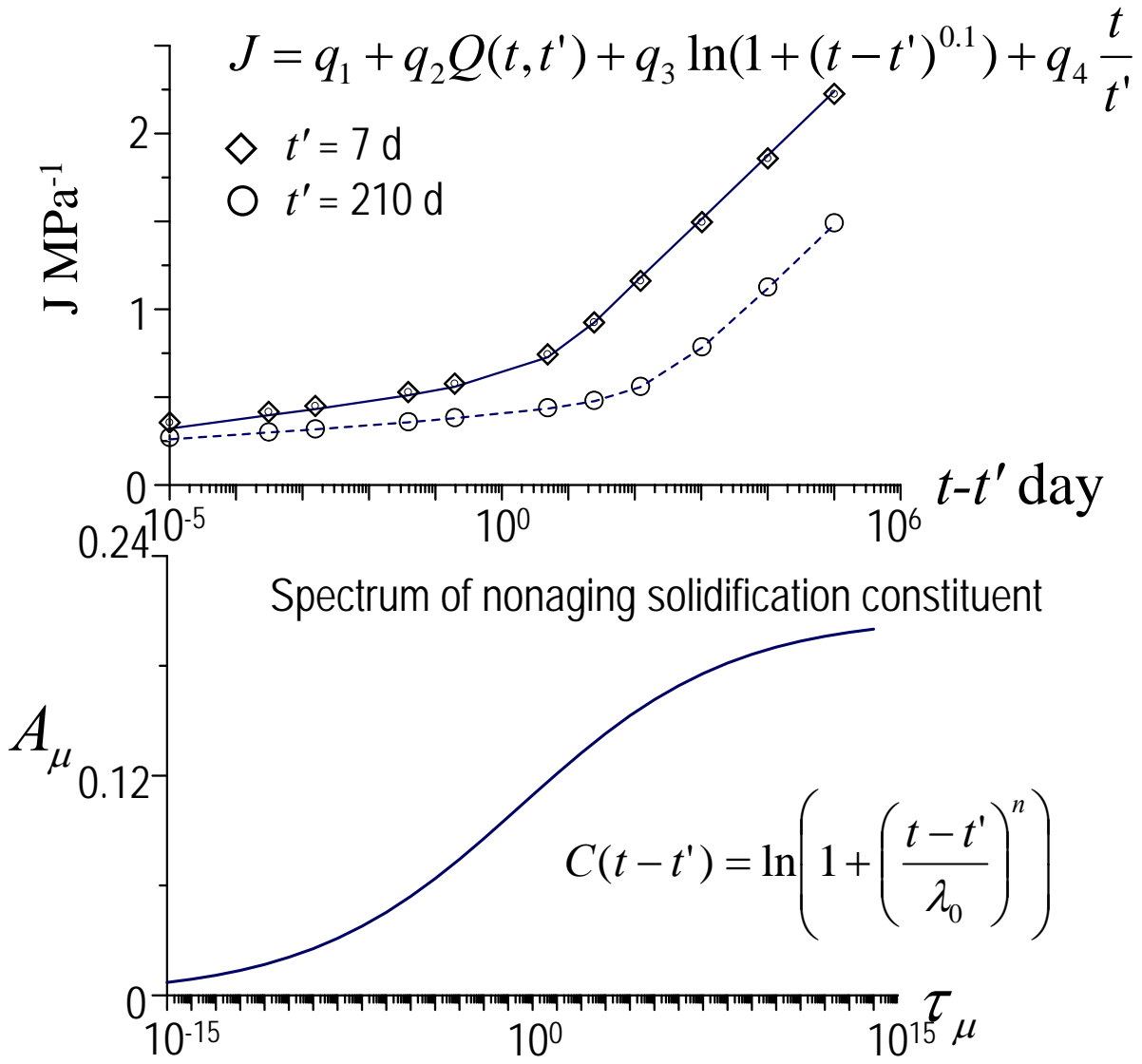
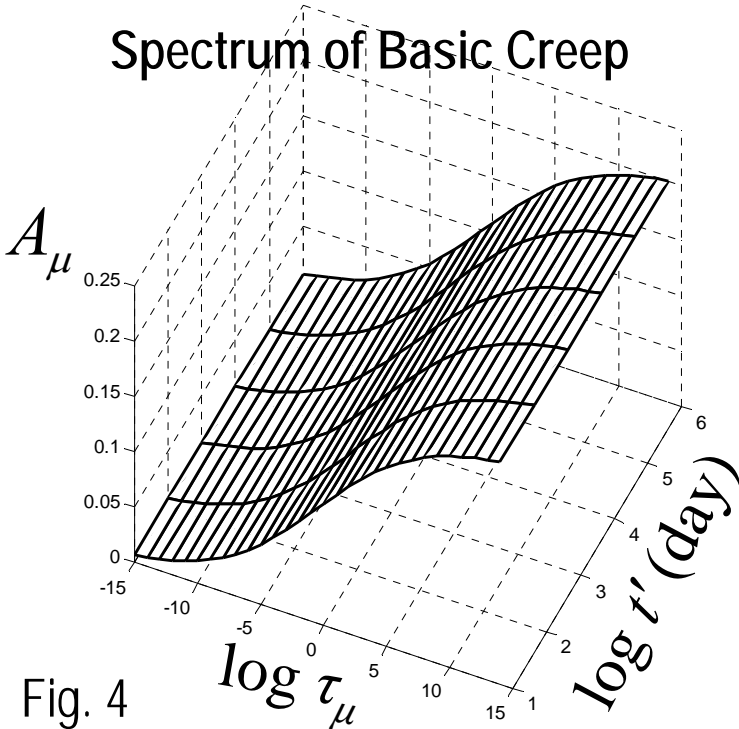


Fig. 3



Spectrum of Basic Creep



Spectrum of Drying Creep

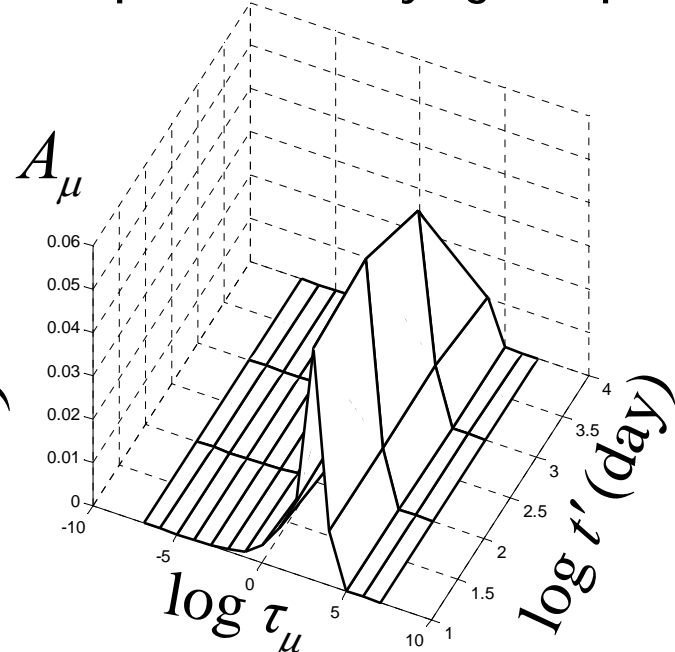


Fig. 4

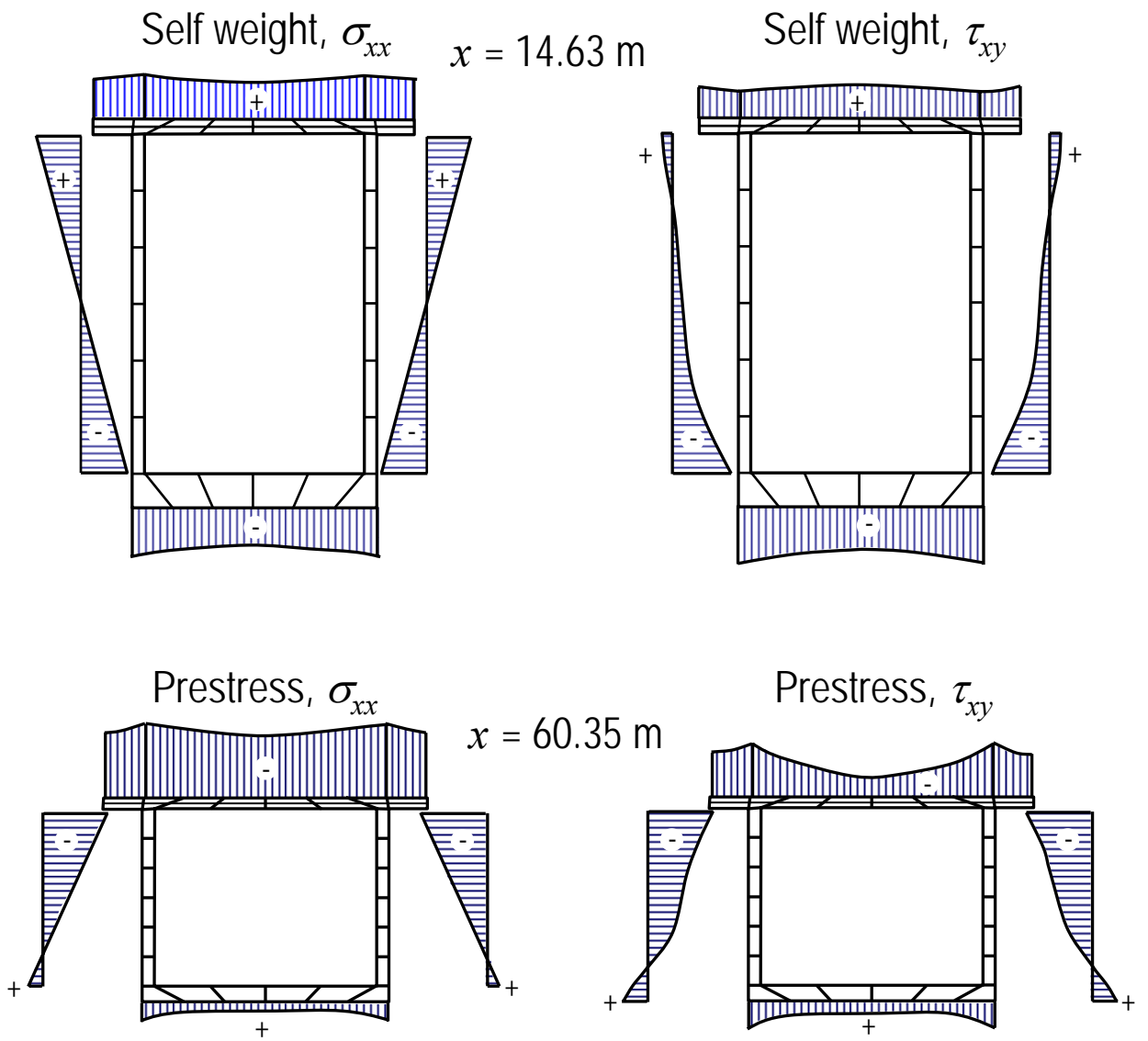


Fig. 5

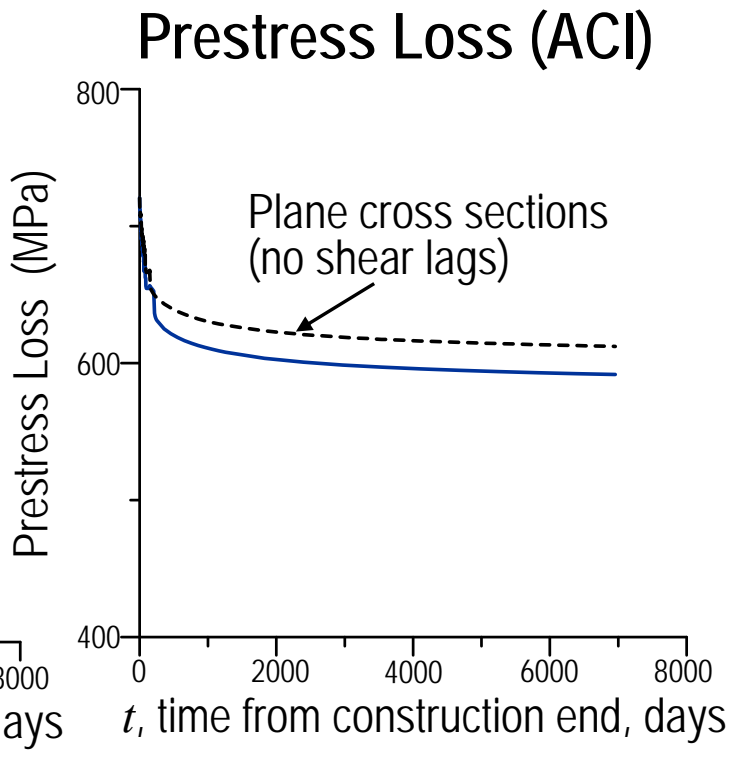
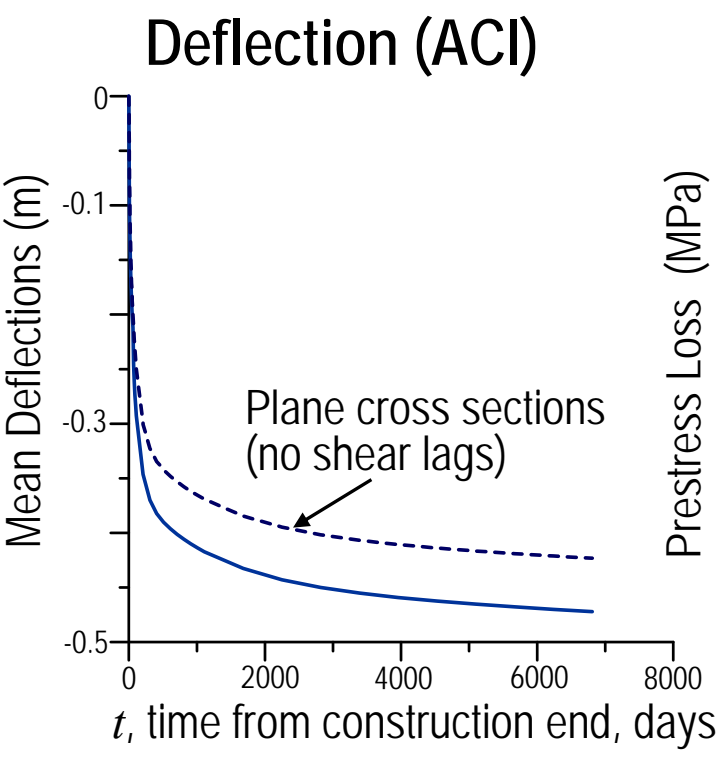
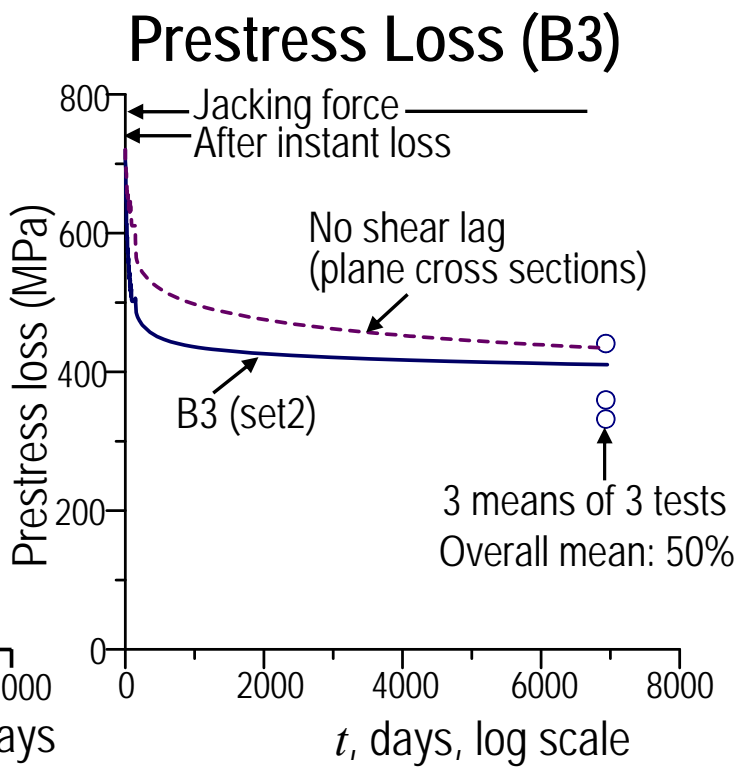
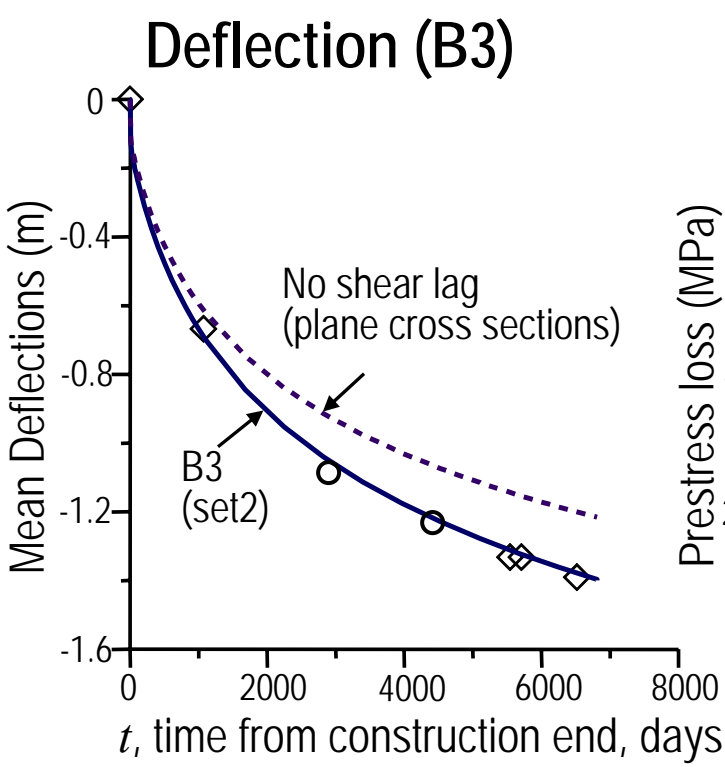


Fig. 6

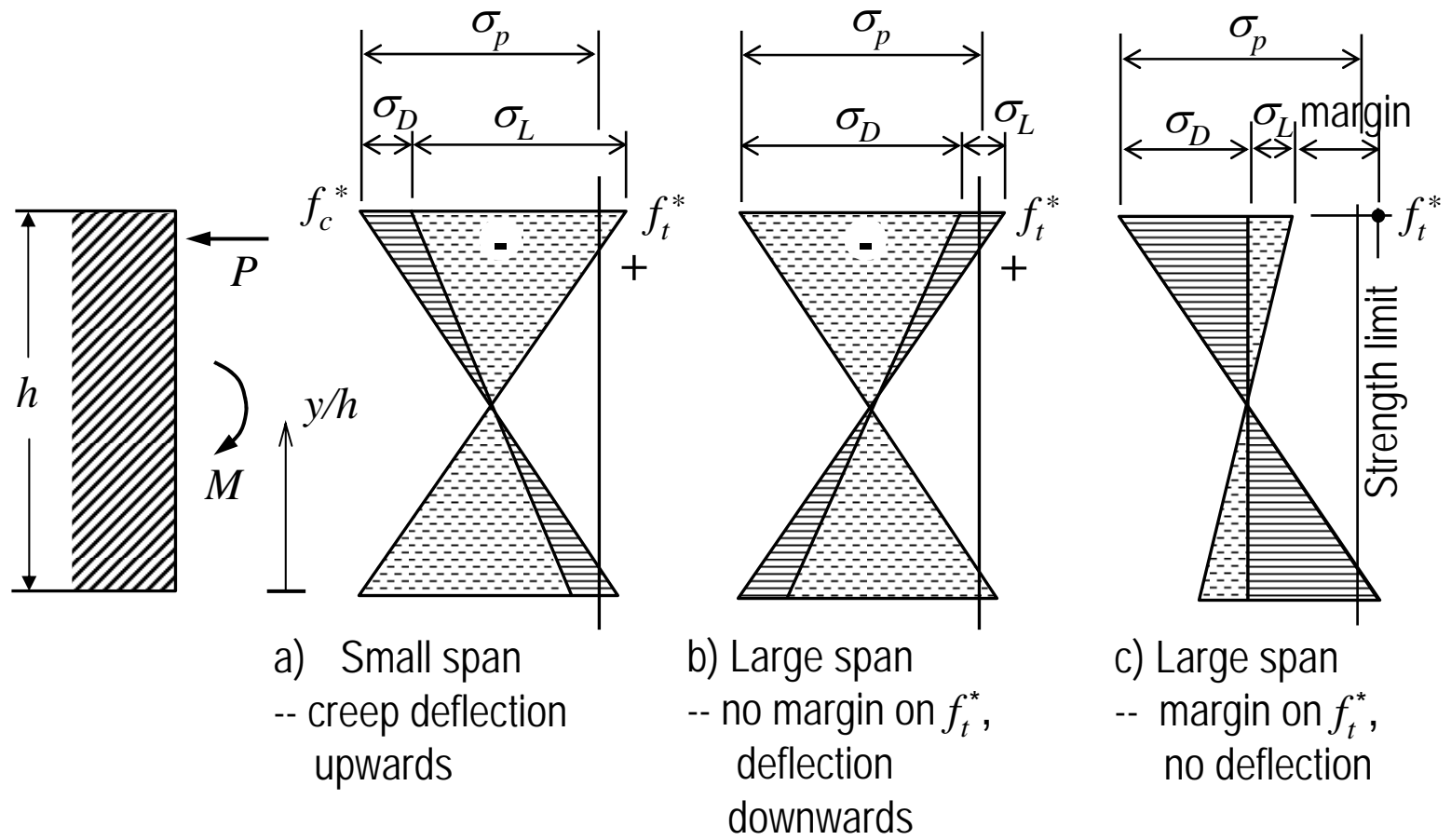


Fig. 7